Engineering Structures 278 (2023) 115496

Contents lists available at ScienceDirect

Engineering Structures

journal homepage: www.elsevier.com/locate/engstruct

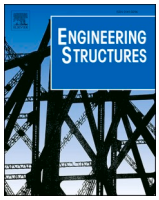

Finite element analysis of reinforced concrete deep beams with square web openings using damage plasticity model

Mona Saleh [a], Mohammad AlHamaydeh [b], Mohamed Zakaria [c,*]

[a] Department of Civil Engineering, Faculty of Engineering, Aswan University, Aswan, Egypt
[b] Department of Civil Engineering, College of Engineering, American University of Sharjah, Sharjah, PO Box 26666, United Arab Emirates
[c] Department of Civil Engineering, Faculty of Engineering, Aswan University , Aswan, Egypt

ARTICLE INFO

Keywords:
Damage plasticity model
Deep beams
Square web openings
Nonlinear behavior
Loading path

ABSTRACT

This study investigates the behavior of RC deep beams with web openings based on the results of numerical simulations using the Abaqus/standard software. The numerical results of the validated specimens showed good agreement with the experimental ones. Then, the proposed concrete damage plasticity (CDP) model was used to examine the effect of various influential parameters, such as the shear span-to-height ratio (a/H), opening size, opening location, concrete compressive strength ($f_c^{'}$), main reinforcement ratio (ρ_s), and web reinforcement ratio (ρ_{web}). It was found that the presence of openings impairs the bearing capacity of RC deep beams, especially openings with sizes of 0.3 and 0.4 of the overall height of the beam. Moreover, openings located through the shear zone significantly reduce the ultimate load, especially on the loading path and near the bearing plates. This is due to the high concentration of shear cracks at the corners of the openings through the loading path line. The behavior of RC deep beams with web openings mainly depends on the openings' size and location. In addition, decreasing the shear span-to-height ratio increases the ultimate load. Meanwhile, increasing the concrete compressive strength ($f_c^{'}$) increases the ultimate load. Similarly, increasing the main reinforcement ratio leads to a higher ultimate load due to adequate cracking control. The same finding can be revealed for the influence of the web reinforcement ratio on the bearing capacity of RC deep beams with web openings. Increasing the main reinforcement ratio from 0.45% to 0.57% and increasing the web reinforcement ratio from 0.29% to 0.33% can enhance the bearing capacity of RC deep beams by 11.36% and 3.26%, respectively. Finally, the numerical investigation reveals that the proposed simulated model can be used to effectively investigate the behavior of RC deep beams with openings overcoming their complexity.

1. Introduction

Recently, openings in RC deep beams became necessary for passing cables and air conditioning or other architectural needs. Openings through the web of RC deep beams lead to stress concentration at the openings' corners and the nonlinear behavior of those beams because the openings through the load transformation to the support point cause an interruption. The significant effect of openings should be considered in studying the nonlinear behavior of RC deep beams. Scientists have considered the behavior of this type of RC member since the 1990s [1-10]. This paper emphasizes the efforts in studying the behavior of RC deep beams with openings, e.g., Abdel-Hakim et al. [11] studied the experimental behavior of RC deep beams with openings with high concrete strength. Sixteen simply-supported deep beams consisting of high- and normal-strength beams were examined under one-point loading. The main parameters considered were the grade of concrete, location, size, shape of web opening, arrangement of reinforcement around web opening, and shear span-to-height ratio. They found that increasing the concrete compressive strength increased the first cracking load and ultimate load. Mainly, the distribution of cracks was affected by the existing openings. The first crack occurred around the opening corners. However, the first cracking load occurred in the beam's flexural zone in beams without opening. Opening interrupting the loading path caused an increase in deflection. Otherwise, the opening shape had an insignificant effect on the deflection. Another study by Hong Guan [12] proposed a model of RC deep beams with openings using the strut-and-tie method. The effects of the opening size, opening location, and shear span-to-height ratio on the ultimate shear strength of eleven tested

* Corresponding author.
E-mail addresses: monaesmail093@gmail.com (M. Saleh), malhamaydeh@aus.edu (M. AlHamaydeh), m.zakaria@aswu.edu.eg (M. Zakaria).

https://doi.org/10.1016/j.engstruct.2022.115496
Received 7 July 2022; Received in revised form 4 December 2022; Accepted 16 December 2022
Available online 28 December 2022

Table 1
Previous studies which investigated the behavior of RC deep beams with openings.

				Studied parameters						
				a/H	Opening characteristics			f_c'	ρ_s	ρ_{web}
	Experimental	Numerical			size	location	shape			
Abdel-Hakim et al. (2004) [11]	√	×	16	√	√	√	√	√	×	×
Guan (2007) [1]	×	√	11	√	√	√	×	×	×	×
O. E. et al. (2007) [2]	√	×	6	√	×	×	×	√	×	×
Tamer et al. (2009) [12]	√	×	13	×	√	√	×	×	×	×
Giuseppe et al. (2012) [4]	√	√	20	×	×	√	×	×	√	√
Haider et al. (2013) [13]	×	√	12	×	×	√	√	×	×	×
HawrazKarim M. Amin et al. [14]	×	√	99	√	√	√	√	√	×	×
Ashraf et al. (2014) [15]	×	√	9	×	×	√	×	×	√	×
Abdul-Razzaq et al. (2017) [5]	√	×	13	√	×	√	√	×	×	×
Ibrahim et al. (2018) [19]	×	√	14	×	√	×	×	√	×	×
Jian Liu (2020) [17]	×	√	27	√	√	×	√	√	×	×
Wen-Yao Lu et al. (2020) [6]	√	×	24	×	√	×	×	√	√	√
Rasha T. S. Mabrouk et al. (2022) [8]	√	√	8	×	√	√	×	×	×	×

beams was numerically examined in this research study. These beams were collected from different experimental sources. They concluded that the strut-and-tie model was affected by the opening size and location. The proposed model was built basically on crack patterns in the experimental studies. Additionally, Hu and Tan [23] experimentally studied the behavior and shear strength of RC deep beams with web openings. Four specimens were tested with various shear span–to–height ratios (0.25 ~ 0.45) and compressive strengths between 35 ~ 44 MPa. The openings in the load passing line from the loading plate to the bearing plate greatly decreased the ultimate shear strength. In addition, specimens with a lower shear span–to–height ratio had the highest ultimate shear strength value. Moreover, Tamer et al. [124] investigated the effect of external shear strengthening around openings of reinforced concrete deep beams using bonded carbon fiber polymer (CFRP). Thirteen specimens with square web openings were experimentally examined under two-point loading. The investigated parameters included the effect of the opening size, location, and presence of CFRP on the ultimate shear strength of the examined deep beams. Their findings also proved the major effect of opening size on the ultimate load. Increasing from 150 mm to 200 mm and from 150 mm to 250 mm caused a decrease in ultimate load by 21 % and 51 %, respectively. Furthermore, Giuseppe et al. [4].

[5] experimentally and analytically investigated the effect of circular openings in reinforced concrete deep beams with a low shear span–to–height ratio (=0.27). Approximately 20 specimens were tested with various reinforcement distributions and opening locations for this study. The study concluded that the opening located in the shear span had the greatest influence on the ultimate load, but the mid-span location was considered ineffective. The horizontal steel was found essential in specimens with openings in the shear span, but vertical steel was determined to be inadequate. Vertical steel was more effective for specimens (with and without openings) in mid-span than horizontal steel. Few studies have also been performed using finite element method (FEM)-based software, e.g., Haider et al. [136] used the ANSYS software to numerically study the effect of opening shape and location on the behavior of RC deep beams with openings. The results showed that the opening location had a much greater effect on the ultimate strength than the opening shape. Additionally, the rectangular opening was found to be better than the other shapes, which had their long sides horizontally extended with the beam span. The best location was the flexural region near the upper corners of the beam. Similarly, HawrazKarim M. Amin et al. [14] numerically investigated the effects of the opening size, opening location, shear span-to-effective depth ratio, maximum aggregate size, and concrete compressive strength using ANSYS + Civil FEM. All examined parameters affected the ultimate shear capacity of the beams. The behavior of the investigated beams was mainly affected by the opening location, especially openings located through the shear zone. Ashraf et al. [157] studied the behavior of RC deep beams (with and without openings) using another finite element method (FEM)-based software named ABAQUS. This study emphasized the effect of the reinforcement distribution on the beam's overall capacity. The main parameters considered were the opening location, reinforcement distribution, simply-supported and continuous beams, and three- and four-point bending. The results showed that the web openings crossing the expected compression struts should be avoided, and the opening depth should not exceed 20 % of the beam's overall depth. Additionally, for simply supported deep beams, the main reinforcement distribution should be 0.1–0.2 of the beam depth. Additionally, Ibrahim et al. [9] used ABAQUS software[9] to investigate the effect of concrete compressive strength and opening size. This study derived a relationship between the studied parameters and the shear strength of RC deep beams with openings. A reduction factor was suggested for beams with similar characteristics and openings as in this study. Then, the reduction factor was multiplied by the *ACI* equation [1610] for deep solid beams to calculate the shear strength of RC deep beams with openings. Even Jian Liu [1711] used the finite element method (FEM) to predict the ultimate shear strength of RC deep beams with web openings. This model was verified against 27 beams from the works of Yang KH et al.[12 18] and EL-Maaddawy et al. [12].[4] The tested beams varied in their concrete compressive strength, opening size, opening shape, and shear span-to-height ratio. The ratio of the experimental shear strength to the predicted shear strength was determined to be approximately 1.03. Abdul-Razzaq et al. [58] used steel plates to strengthen the openings in RC deep beams. This new technique was experimentally tested on 13 specimens under the four-point bending of RC deep beams with square, circular, and rectangular openings. The effect of the opening shape strengthened with steel plates and the effect of using stud connectors were examined. Then, the effects of the shear span-to-height ratio, opening size, steel plate thickness, and number of stud connectors on the strength and behavior of the tested specimens were experimentally analyzed. Wen-Yao Lu et al. [613] tested 24 specimens with square openings. This study examined the influence of the concrete compressive strength, opening size, web reinforcement in the horizontal direction, and main reinforcement ratio. Rasha T. S. Mabrouk et al. [8] experimentally and numerically studied the effect of the opening size and location. They found that openings with small sizes did not significantly affect the behavior of the tested beams. Nonetheless, large openings showed remarkable influence, especially in varying the opening locations. Table 1 summarizes the aforementioned.

Moreover, Jithinbose K J et al. [20] presented a review of studies that investigated the issue of openings in beams, including deep beams, which were [21,22,18,23,24,12,4,13], and [15]. Most of those studies concentrated on the opening size and opening location.

All of these previous studies had limitations and uncertainties in

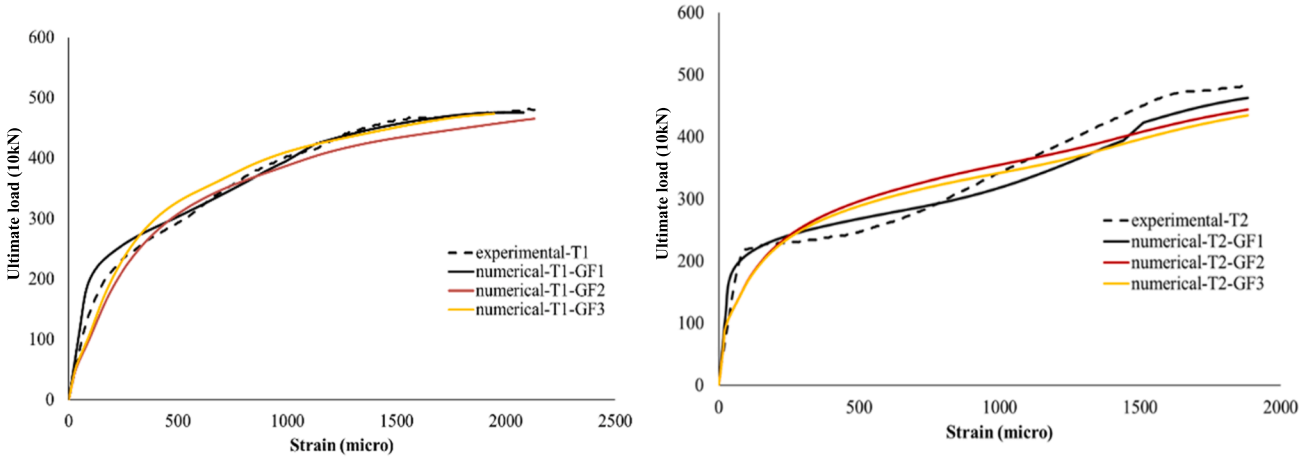

a) Fracture energy calibration for specimen B1

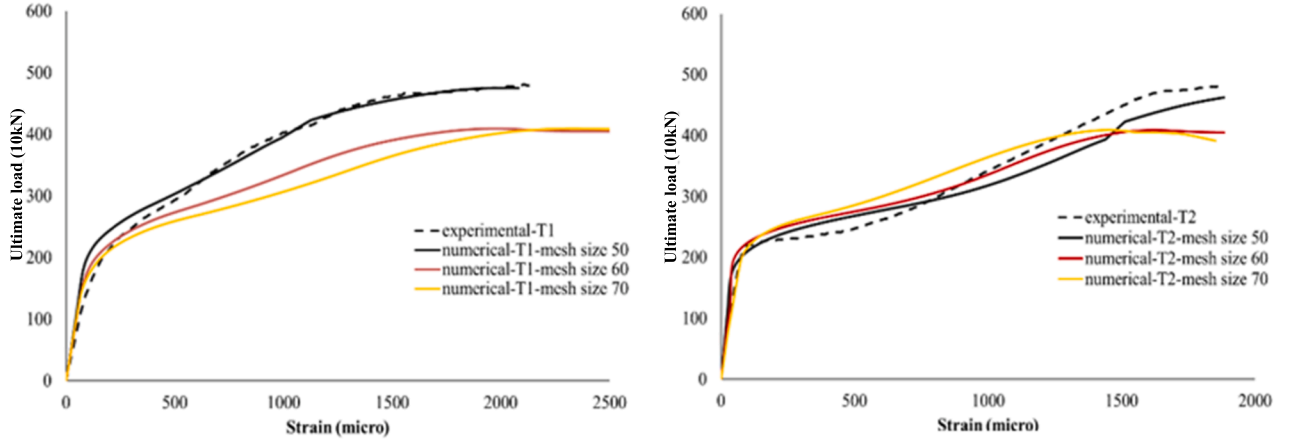

b) Mesh sensitivity for specimen B1

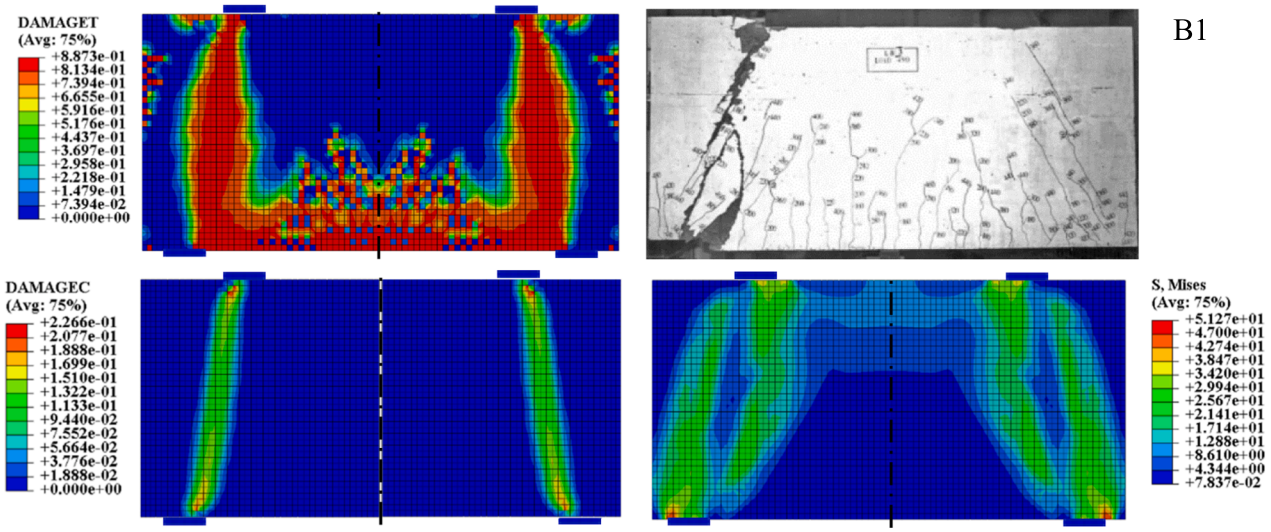

Fig. 1. Results of the validated beams [2].

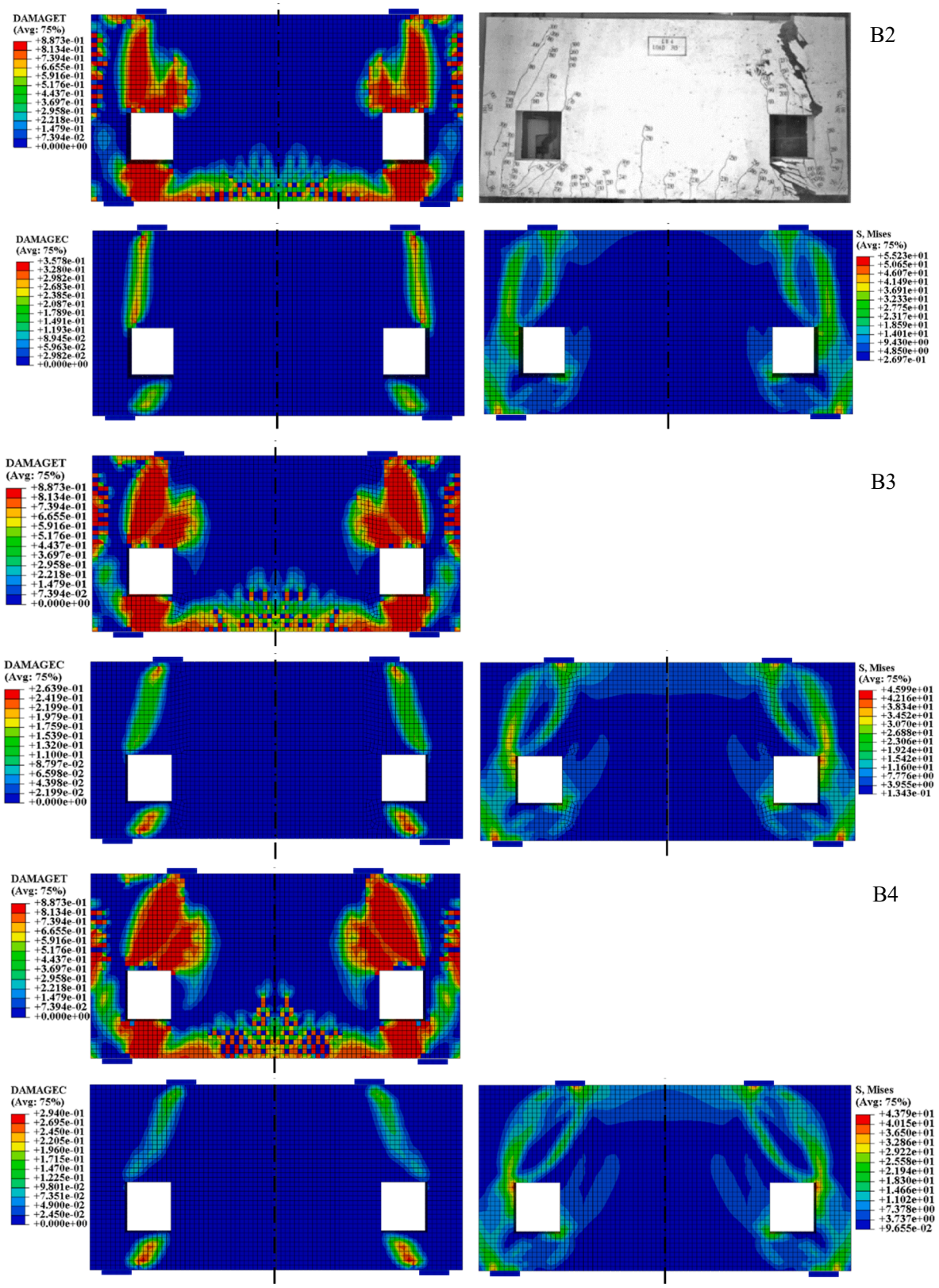

c) Crack patterns for specimens B1, B2, B3, and B4.

Fig. 1. (*continued*).

Table 2
Material properties and results of verified beams [2].

Reference Name	Current Name	Material properties						Ultimate loads of best results				
		f'_c MPa	f_{ys} MPa	f_{yh}, f_{yv} MPa	ρ_s(%)	ρ_h(%)	ρ_v(%)	P_u (experimental) kN	P_u (numerical) kN	$\mu = \frac{P_{u(experimental)}}{P_{u(numerical)}}$	Mean	SD
LB3	B1	38.6	537.4	541.6	0.61	0.2	0.2	4900	4755.55	1.030	0.981	0.04
LB4	B2	38.6	537.4	541.6	0.61	0.4	0.3	3150	3257.51	0.967		
LB5	B3	43.9	537.4	541.6	0.61	0.4	0.3	2700	2720.42	0.992		
LB6	B4	34.3	537.4	541.6	0.61	0.4	0.3	2000	2137.55	0.936		

Where ρ_s: main reinforcement ratio $= \frac{A_s}{bh}$

ρ_h: horizontal web reinforcement ratio $= \frac{A_{sv}}{S_v b}$

ρ_v: vertical web reinforcement ratio $= \frac{A_{sh}}{S_h b}$

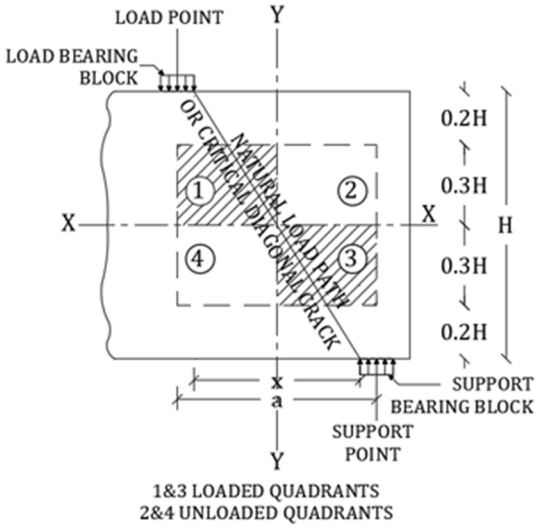

Fig. 2. Practical region for web opening (Proposed by Ray and Reddy, 1979; Ray, 1980; 1982) [34].

explaining the behavior and failure modes of RC deep beams, especially if there were web openings. Most studies did not consider the effect of the shear span-to-height ratio, concrete compressive strength, main reinforcement ratio, and web steel. Therefore, this paper considers all effective parameters. Initially, specimens from the literature were selected and analyzed to validate the capability of using the concrete damage plasticity model (CDPM) provided in Abaqus/standard to predict the behavior of RC deep beams. Then, a dataset of the numerical work was established on simply-supported RC deep beams with web openings.

2. Research significance

The nonlinear behavior of structural bending members such as deep beams has been experimentally studied; however, those studies were mostly limited to small-scale specimens of deep concrete beams, which may not be the case that expresses the behavior of real beams. In addition, conducting experimental tests on large beams requires more time, human force, cost, and capability of specimen corruption during the test. Thus, using computer-based software such as ABAQUS to numerically study reinforced concrete deep beams is beneficial. Therefore, this paper uses the ABAQUS software to numerically analyze reinforced concrete deep beams and implement assumptions for many more real cases with more specimens. The current study investigates the behavior of reinforced concrete deep beams with square web openings. To achieve this goal, first, specimens from the literature were selected and analyzed to validate the capability of using the concrete damage plasticity (CDP) model provided in Abaqus/standard to predict the behavior of RC deep beams. Next, a dataset of the numerical work was established on simply-supported RC deep beams with web openings. Three hundred and seventy-two specimens were simulated to examine the effect of the various influential parameters on the ultimate strength, load versus mid-span deflection response, and crack pattern; the influential parameters included the shear span-to-height ratio (a/H), opening size, opening location, concrete compressive strength (f'_c), main reinforcement ratio (ρ_s), and web reinforcement ratio (ρ_{web}).

3. Validation

To study the capability of using numerical programs to predict RC deep beams' behavior, large-scale deep beams' simulations have been numerically analyzed using the concrete damage plasticity model (CDPM). The concrete compression curve is represented in Eq. (1), which was proposed by C. A. Coronado and M. M. Lopez [25]. The concrete tension curve is represented in Eq. (2), which is given by *ACI* 318–05 [26].

$$\sigma_c = 1.8 * f'_c \left(\frac{\frac{\varepsilon_c}{\varepsilon_o}}{1 + \left(\frac{\varepsilon_c}{\varepsilon_o}\right)^2} \right) \tag{1}$$

$$\frac{\sigma_t}{f_{ct}} = \left[1 + \left(c_1 \frac{w}{w_{cr}} \right)^3 \right] e^{\left(-c_2 \frac{w}{w_{cr}} \right)} - \frac{w}{w_{cr}} \left(1 + c_1^3 \right) e^{(-c_2)} \tag{2}$$

where σ_c is the concrete compressive stress; ε_c is the strain; $\varepsilon_o = \frac{2f'_c}{E_c}$; f'_c is the specified compressive strength of concrete; E_c is the concrete modulus of elasticity, and $E_c = 4700\sqrt{f'_c}$ in MPa ; σ_t is the tensile stress normal to the crack direction; $f_{ct} = 0.6\sqrt{f'_c}$; f_{ct} is the average splitting tensile strength of concrete; c_1 and c_2 are constants with values of 3 and 6.93, respectively, and can be determined based on tensile tests of the concrete. w is the crack opening displacement, and w_{cr} is the cracking width where the tensile strength has completely vanished $w_{cr} = 5.14 G_f / f_{ct}$. The fracture energy ($G_f$) can be obtained using Eq. (3) [27], Eq. (4) [25], and Eq. (5) [28]:

$$G_{fI} = \begin{cases} G_{fo} \left(\frac{f'_c}{10} \right)^{0.7} & if f'_c \le 80MPa \\ 4.3 G_{fo} & if f'_c > 80MPa \end{cases} \tag{3}$$

$$G_{fII} = 2.5 \alpha_o \left(\frac{f'_c}{0.051} \right)^{0.46} \left(1 + \frac{d_a}{11.27} \right)^{0.22} wc^{-0.3} \tag{4}$$

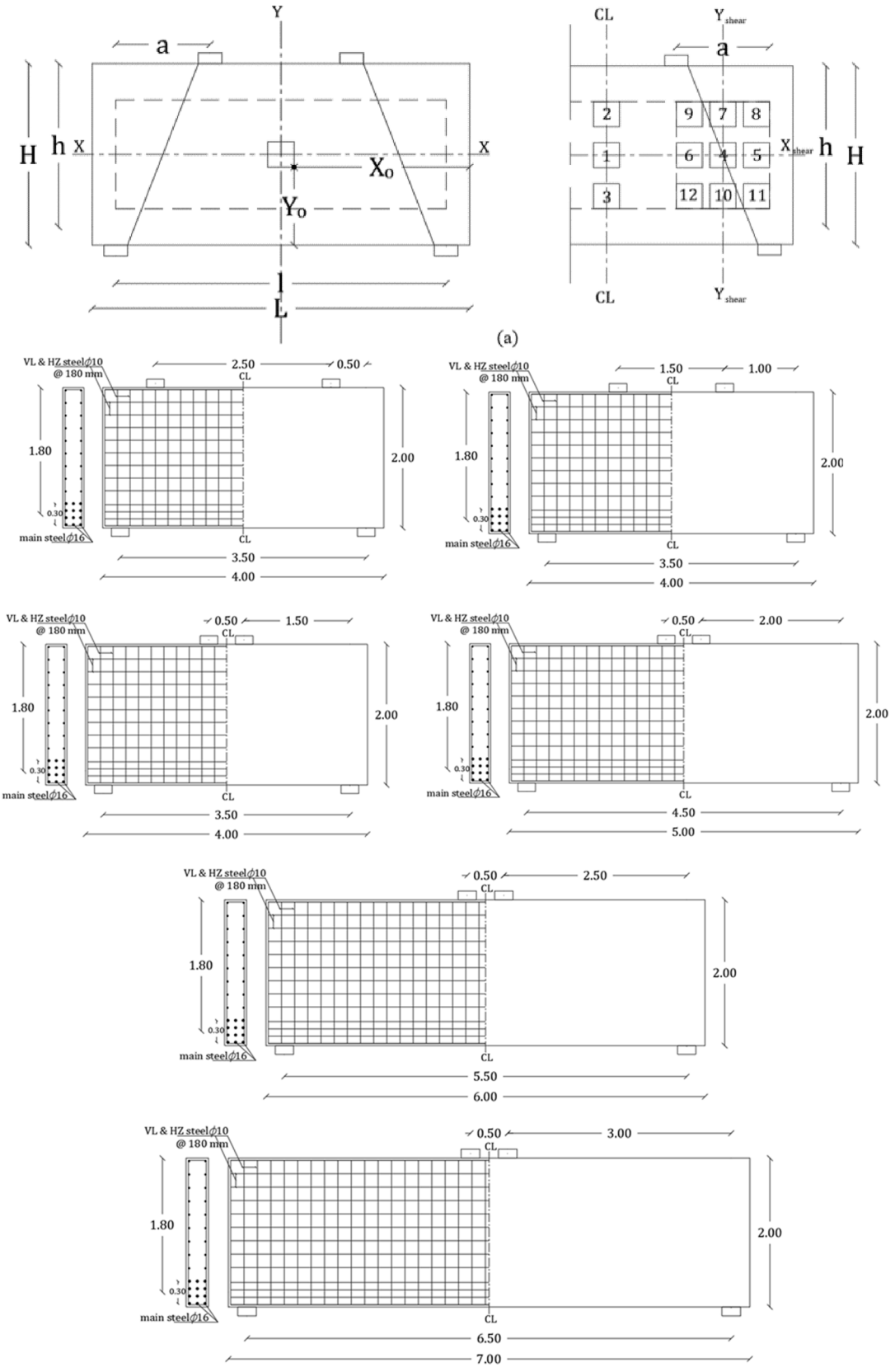

Fig. 3. A) notations of the tested beams; b) details of reference deep beams without openings - all dimensions are in (m).

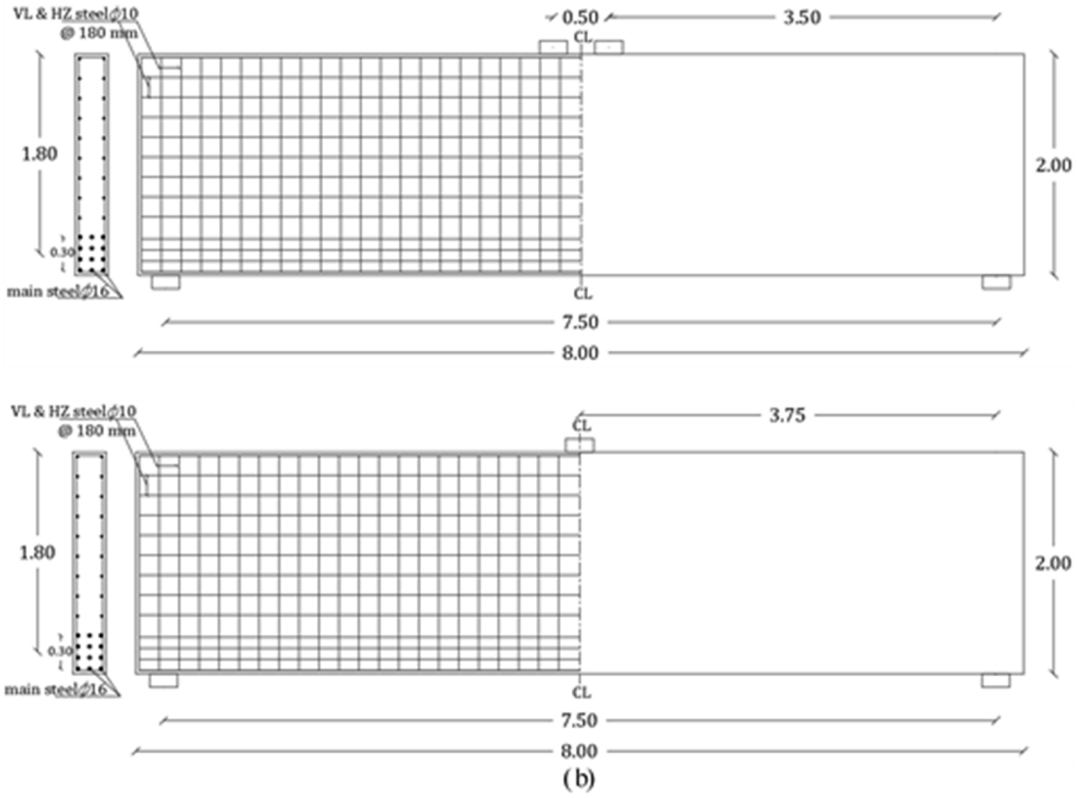

Fig. 3. (*continued*).

$$G_{fIII} = \left(0.0469 d_{max}^{2} - 0.5 d_{max} + 26\right)\left(\frac{f_c^{'}}{10}\right)^{0.7} \quad (5)$$

where G_{fo} is the reference fracture energy, whose values are 0.025, 0.03, and 0.058 for a maximum aggregate size d_{max} of 8, 16, and 32, respectively; $\alpha_0 = 1.44$ (for crushed or angular aggregate). d_a is the aggregate diameter in mm. w_c is the water-cement ratio of the concrete mix.

Moreover, while defining the tension-softening behavior of concrete in Abaqus, there are two main options:

- Fracture energy criterion, which uses the stress-cracking displacement data.
- Material softening behavior, which uses the stress-cracking strain data.

The fracture energy criterion used in the current study depends on the energy required to open a unit area of the crack (G_f). This energy is a material property that is not dependent on the mesh element size [29,30,31,32]. Then, the model was calibrated with three fracture energy equations. The calibration results showed that Eq. (3) [27] was more accurate than the other examined equations. The results of the three equations are presented in Fig. 1 (a).

Other defined parameters in the CDP model are the dilation angle (ψ), eccentricity (ϵ), biaxial/uniaxial compression plastic strain ratio (fb_0/fc_0), ratio of the second stress invariant on the tensile meridian (K), and viscosity parameter (μ). [1819]The previous parameters have been tested on large deep beams (B1, B2, B3, and B4) studied by Hu and Tan [2].

The recommendation from ABAQUS for the dilation angle appears too small for reinforced concrete (RC) deep beams. So, many researchers studied the sensitivity of dilation angle in numerical simulation of RC deep beams, and they found that the small values of dilation angle exhibit very brittle behavior with very low ultimate load capacity [33]. So, a higher value is needed to establish an accurate numerical model. So, the recommended values of these parameters are 54°, 0.1, 1.16, 0.667, and 0.001 for ψ, ϵ, fb_0/fc_0, K, and μ, respectively. Moreover, validation was examined by choosing mesh sizes of 50, 60, and 70 mm. Decreasing the mesh size increases the accuracy of the numerical results. The load–strain curve for both ABAQUS results using values of calibrated CDPM parameters and experimental results is given in Fig. 1 (b). The ultimate loads are compared in Table 2 for the experimental and numerical specimens. Crack patterns are compared in Fig. 1 (c) for experimental specimens versus specimens tested by ABAQUS software. Fig. 1 (c) clearly shows that the cracks occur in the same positions and with the same trajectory for experimental tests and numerical specimens examined by the ABAQUS software.

4. Numerical program

The study was conducted on RC deep beams with rectangular cross-sections under two-point symmetric top-loading to examine the effect of the following parameters: shear span-to-height ratio (a/H), opening size, opening location, compressive strength of concrete ($f_c^{'}$), main reinforcement ratio (ρ_s), and web reinforcement ratio (ρ_{web}). To investigate the effect of openings on the tested beams, reference beams without openings were simulated. Opening locations varied through the flexural zone and shear zone. Ray and Reddy suggested a practical region for web openings called the shear zone, as shown in Fig. 2 [34].

4.1. Geometrical properties of deep beams

To achieve the objective of this paper, 372 rectangular cross-section concrete deep beams were analyzed. All tested simply-supported beams had a constant breadth of 300 mm, a total length of 4000 mm, and an overall height of 2000 mm. For all tested beams, the dimensions of the loading and bearing plates were 250 mm in length, 300 mm in width, and 20 mm in thickness. The program of the current study contains six series as follows:

Table 3
Opening characteristics of the tested beams.

Opening size (mm)	Specimen	Location	X_o(mm)	Y_o(mm)	Specimen	Location	X_o(mm)	Y_o(mm)	Specimen	Location	X_o(mm)	Y_o(mm)
	G1($a/H = 0.25$)				G2 ($a/H = 0.5$)			G3 ($a/H = 0.75$)				
0	G1-Ozero	–	0	0	G2-Ozero	–	0	0	G3-Ozero	–	0	0
400	G1-O4-1	mid span	1800	800‘	G2-O4-1	mid span	1800	800	G3-O4-1	mid span	1800	800
	G1-O4-2		1800	1200	G2-O4-2		1800	1200	G3-O4-2		1800	1200
	G1-O4-3		1800	400	G2-O4-3		1800	400	G3-O4-3		1800	400
	G1-O4-4	Shear Zone	300	800	G2-O4-4	Shear Zone	550	800	G3-O4-4	Shear Zone	800	800
	G1-O4-5		250	800	G2-O4-5		250	800	G3-O4-5		250	800
	G1-O4-6		350	800	G2-O4-6		850	800	G3-O4-6		1350	800
	G1-O4-7		300	1200	G2-O4-7		550	1200	G3-O4-7		800	1200
	G1-O4-8		250	1200	G2-O4-8		250	1200	G3-O4-8		250	1200
	G1-O4-9		350	1200	G2-O4-9		850	1200	G3-O4-9		1350	1200
	G1-O4-10		300	400	G2-O4-10		550	400	G3-O4-10		800	400
	G1-O4-11		250	400	G2-O4-11		250	400	G3-O4-11		250	400
	G1-O4-12		350	400	G2-O4-12		850	400	G3-O4-12		1350	400
600	G1-O6-1	mid span	1700	700	G2-O6-1	mid span	1700	700	G3-O6-1	mid span	1700	700
	G1-O6-2		1700	1000	G2-O6-2		1700	1000	G3-O6-2		1700	1000
	G1-O6-3		1700	400	G2-O6-3		1700	400	G3-O6-3		1700	400
	G1-O6-5	Shear Zone	250	700	G2-O6-4	Shear Zone	450	700	G3-O6-4	Shear Zone	700	700
	G1-O6-8		250	1000	G2-O6-5		250	700	G3-O6-5		250	700
	G1-O6-11		250	400	G2-O6-6		650	700	G3-O6-6		1150	700
					G2-O6-7		450	1000	G3-O6-7		1000	700
					G2-O6-8		250	1000	G3-O6-8		1000	250
					G2-O6-9		650	1000	G3-O6-9		1000	1150
					G2-O6-10		450	400	G3-O6-10		400	700
					G2-O6-11		250	400	G3-O6-11		400	250
					G2-O6-12		650	400	G3-O6-12		400	1150
800	G1-O8-1	mid span	1600	600	G2-O8-1	mid span	1600	600	G3-O8-1	mid span	1600	600
	G1-O8-2		1600	800	G2-O8-2		1600	800	G3-O8-2		1600	800
	G1-O8-3		1600	400	G2-O8-3		1600	400	G3-O8-3		1600	400
	G1-O8-5	Shear Zone	250	600	G2-O8-4	Shear Zone	350	600	G3-O8-4	Shear Zone	600	600
	G1-O8-8		250	800	G2-O8-5		250	600	G3-O8-5		250	600
	G1-O8-11		250	400	G2-O8-6		450	600	G3-O8-6		950	600
					G2-O8-7		350	800	G3-O8-7		800	600
					G2-O8-8		250	800	G3-O8-8		800	250
					G2-O8-9		450	800	G3-O8-9		800	950
					G2-O8-10		350	400	G3-O8-10		400	600
					G2-O8-11		250	400	G3-O8-11		400	250
					G2-O8-12		450	400	G3-O8-12		400	950
	G4($a/H = 1$)				G5 ($a/H = 1.25$)			G6 ($a/H = 1.5$)				
0	G4-Ozero	–	0	0	G5-Ozero	–	0	0	G6-Ozero	–	0	0
400	G4-O4-4	Shear Zone	1050	800	G5-O4-4	Shear Zone	1300	800	G6-O4-4	Shear Zone	1550	800
	G4-O4-7		1050	1200	G5-O4-7		1300	1200	G6-O4-7		1550	1200
	G4-O4-9		1850	1200	G5-O4-9		2350	1200	G6-O4-9		2850	1200
	G4-O4-10		1050	400	G5-O4-10		1300	400	G6-O4-10		1550	400
	G4-O4-11		250	400	G5-O4-11		250	400	G6-O4-11		250	400
	G7($a/H = 1.75$)				G8 ($a/H = 2$)							
0	G7-Ozero	–	0	0	G8-Ozero	–	0	0				
400	G7-O4-4	Shear Zone	1800	800	G8-O4-4	Shear Zone	2050	800				
	G7-O4-7		1800	1200	G8-O4-7		2050	1200				
	G7-O4-9		3355	1200	G8-O4-9		3850	1200				
	G7-O4-10		1800	400	G8-O4-10		2050	400				
	G7-O4-11		250	400	G8-O4-11		250	400				

Note: dimensions of the loading and bearing plates were 250 mm in length, 300 mm in width, and 20 mm in thickness.

Series 1 contains 99 specimens with identical cylinder compressive concrete strength ($f_c^{'} = 32\,\mathrm{N/mm^2}$), main reinforcement ratio$\rho_s = 0.45$ %, and web reinforcement ratio$\rho_{web} = 0.29$ %. This series was divided into three groups. Each group had a different shear span-to-height ratio. The selected values of the shear span-to-height ratio (a/H) were 0.25 for Group 1 (G1), 0.5 for Group 2 (G2), and 0.75 for Group 3 (G3). Three square opening sizes were tested to examine the effect of the opening size on the ultimate shear strength: 400 mm, 600 mm, and 800 mm. Additionally, to examine the effect of the opening location, 12 opening locations were tested, and they varied between three opening locations in the flexural zone and nine opening locations in the shear zone.

Series 2 contains 99 specimens with identical cylinder compressive concrete strength ($f_c^{'} = 40\,\mathrm{N/mm^2}$), main reinforcement ratio$\rho_s = 0.45$ %, and web reinforcement ratio$\rho_{web} = 0.29$ %. Similar to series 1, this series was also divided into three groups with different shear span-to-height ratios (a/H): 0.25 for Group 1 (G1), 0.5 for Group 2 (G2), and 0.75 for Group 3 (G3). Three square opening sizes (400 mm, 600 mm, and 800 mm) were tested to examine the effect of opening size on the ultimate shear strength. Additionally, to examine the effect of the opening location, 12 opening locations were tested, with three opening locations in the flexural zone and nine opening locations in the shear zone. Additionally, five groups were simulated with larger shear span-to-height ratios (a/H). Each group had six specimens, a solid reference beam, and five beams with openings (locations 4, 7, 9, 10, and 11). The tested shear span-to-height ratios (a/H) were 1 for G4, 1.25 for G5, 1.5 for G6, 1.75 for G7, and 2 for G8.

Series 3 contains 99 specimens with identical cylinder compressive concrete strength ($f_c^{'} = 48\,\mathrm{N/mm^2}$), main reinforcement ratio$\rho_s = 0.45$ %, and web reinforcement ratio$\rho_{web} = 0.29$ %. Similar to series 1 and 2, series 3 was divided into three groups based on their shear span-to-height ratio (a/H): Group 1 (G1) with $a/H = 0.25$, Group 2 (G2) with $a/H = 0.5$, and Group 3 (G3) with $a/H = 0.75$. Three square opening

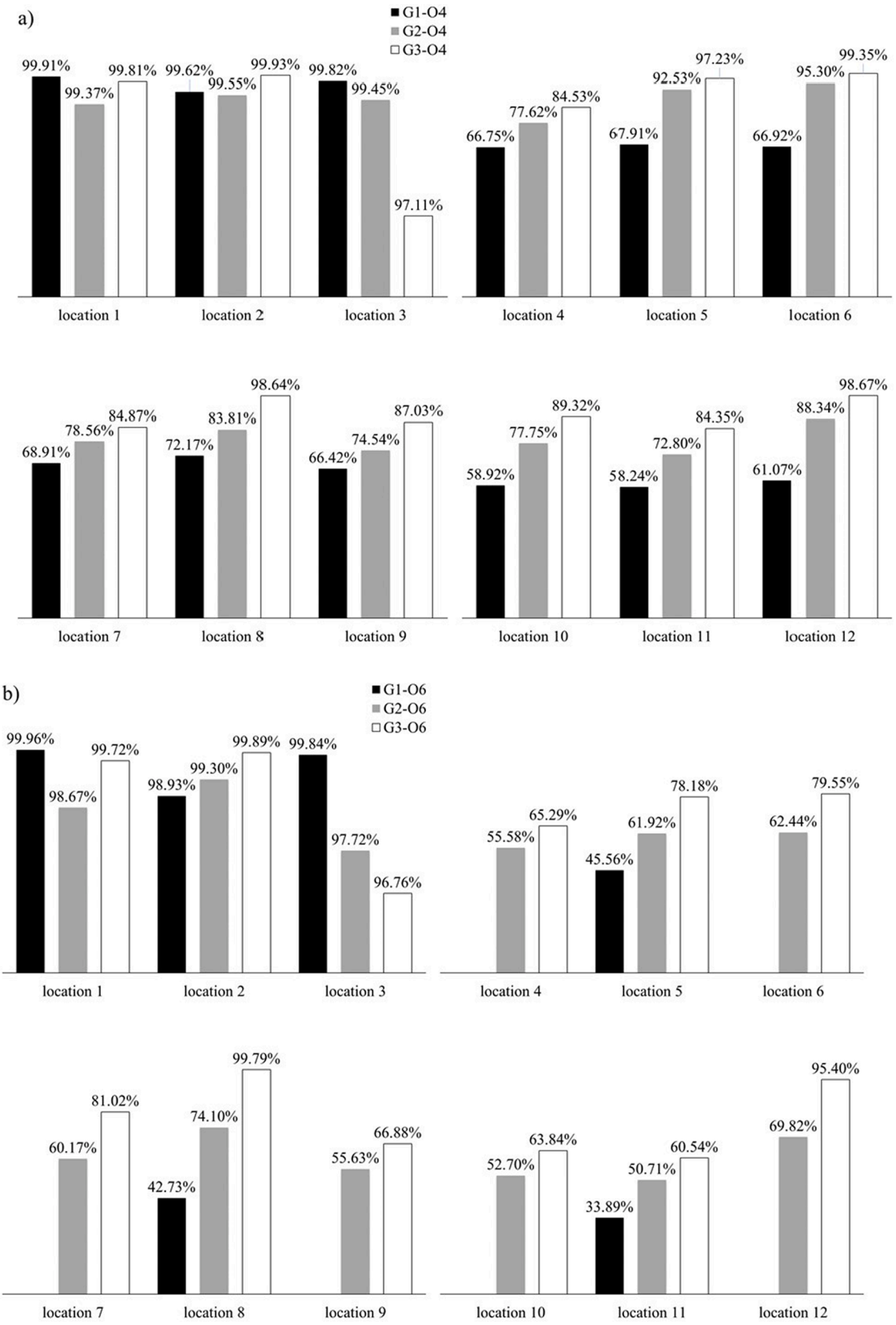

Fig. 4. Ultimate load of beams with openings to solid beam series 1.a). Beams with an opening size of 400 mm (0.2H). b). Beams with an opening size of 600 mm (0.3H). c). Beams with an opening size of 800 mm (0.4H).

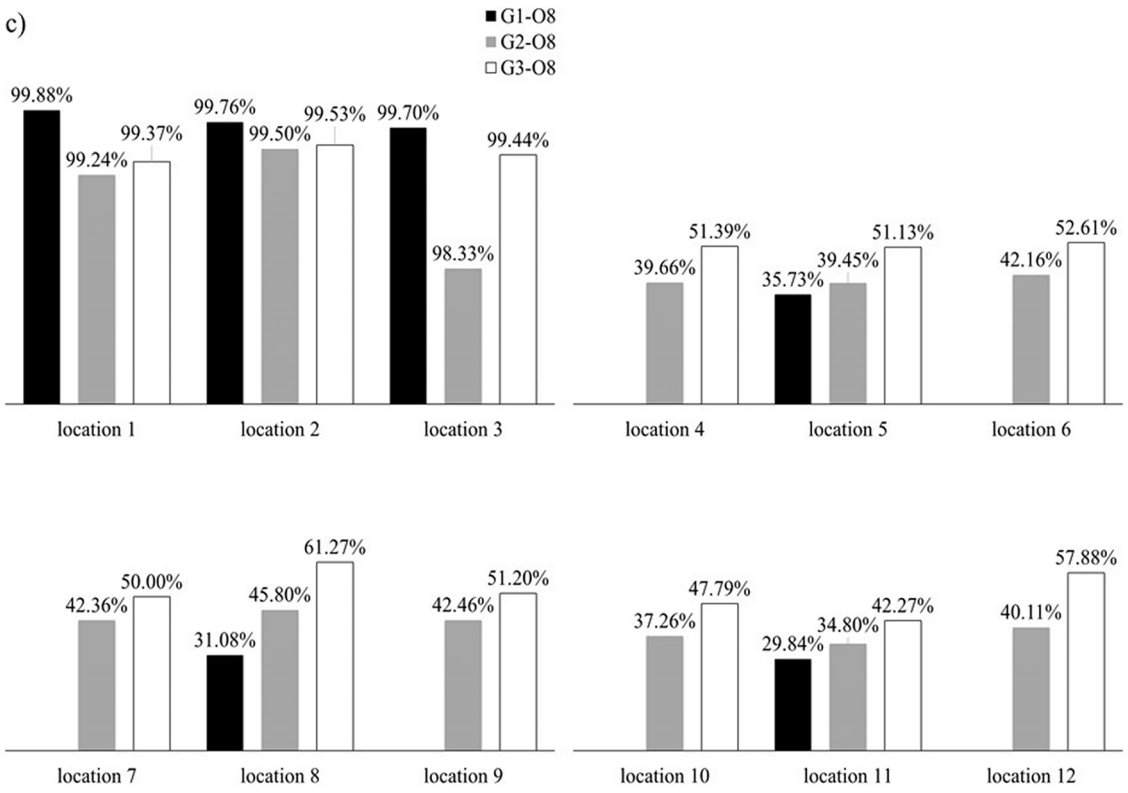

Fig. 4. (*continued*).

sizes (400 mm, 600 mm, and 800 mm) were also tested to examine the effect of the opening size on the ultimate shear strength and the effect of the opening location. Twelve opening locations were tested, consisting of three opening locations in the flexural zone and nine in the shear zone.

Series 4 contains 20 specimens with identical cylinder compressive concrete strength ($f_c^{'} = 40\,\mathrm{N/mm^2}$). Five deep beams were selected with critical opening locations in the shear zone. The beams from series 2, G2-O4, were considered reference beams with the main reinforcement ratio (ρ_s) of 0.45 %. Four ratios were simulated to examine the effect of the main reinforcement ratio variation: 0.21 %, 0.25 %, 0.33 %, and 0.57 %. The ratios of 0.21 % and 0.33 % varied in (h) effective depth, which were 1900 mm and 1850 mm, respectively. The ratios of 0.25 % and 0.57 % varied in diameter of the bars, which were $\varnothing 12\,\mathrm{mm}$ and $\varnothing 18\,\mathrm{mm}$, respectively.

Series 5 contains 15 specimens with identical cylinder compressive concrete strength ($f_c^{'} = 40\,\mathrm{N/mm^2}$). Five deep beams were selected with critical opening locations in the shear zone. The beams from series 2, G2-O4, were considered the reference beams with a web reinforcement ratio (ρ_{web}) of 0.29 %. To examine the effect of web reinforcement ratio variation, three ratios were simulated: ρ_{web}= 0.24 %, 0.26 %, and 0.33 %, with vertical and horizontal distances between web bars of 220 mm, 200 mm, and 160 mm, respectively. According to the Egyptian code [35], the vertical and horizontal distances should not exceed 200 mm. However, a distance of 220 mm was used in this study to examine the effect of different ratios on the ultimate load of the tested beams.

For all studied beams, the clear spacing between the main bars was 100 mm, and the distance between the bottom cover and the main bars was 30 mm. All beams were provided with web reinforcement constituting a $\varnothing 10\,mm$ bar. Complete details of the reinforcement and geometric aspects for the analyzed beams are illustrated in Fig. 3 and Table 3.

To simplify, a system of nomenclature was used for the beams and is given as follows:

G1-O4-1

The first letter G1 denotes the specimen group, which is used for theoretical investigation and signifies the shear span-to-height ratio (a/H). As mentioned, G1 has a shear span-to-height ratio (a/H) of 0.25, while G2 and G3 have shear span-to-height ratios (a/H) of 0.5 and 0.75, respectively. Next, with the separator, O4 denotes the opening size (Ozero, O4, O6, and O8 were used for beams without openings, an opening size of 400 mm, 600 mm, and 800 mm, respectively). Then, the numeric order of the parametric model is followed by a separator referring to the opening location, as shown in Fig. 3 (a). The position of the opening with respect to the edge of the beam is shown in Fig. 3 (a).

To verify the other studied beams in series 4, 5, and 6, the following nomenclature was used:

S4-O4-4

S4 refers to the series number, O4 denotes the opening size, and the numeric order of the parametric model is followed by a separator referring to the opening location.

where L is the specimen total length.

l: specimen clear span.

H: specimen overall height.

h: specimen effective depth.

b: specimen breadth.

a: specimen shear span.

X_o: distance of the opening bottom corner to the edge of the beam in the x-direction.

Y_o: distance of the opening bottom corner to the edge of the beam in the y-direction.

a/H: shear span-to-height ratio.

5. Results

The numerical results include the ultimate strength, load versus mid-

Table 4
Numerical results of the tested beams in series 1.

Group	G1($a/H = 0.25$)			G2 ($a/H = 0.5$)			G3 ($a/H = 0.75$)		
Opening size (mm)	Specimen Name	P_u(kN)	P_{uo}/P_{us}	specimen Name	P_u(kN)	P_{uo}/P_{us}	specimen Name	P_u(kN)	P_{uo}/P_{us}
zero	G1-Ozero	6436.393	100 %	G2-Ozero	3930.046	100 %	G3-Ozero	2918.360	100 %
0.2H = 400	G1-O4-1	6430.608	99.91 %	G2-O4-1	3905.321	99.37 %	G3-O4-1	2912.888	99.81 %
	G1-O4-2	6411.763	99.62 %	G2-O4-2	3912.454	99.55 %	G3-O4-2	2916.454	99.93 %
	G1-O4-3	6425.016	99.82 %	G2-O4-3	3908.549	99.45 %	G3-O4-3	2834.113	97.11 %
	G1-O4-4	4296.265	66.75 %	G2-O4-4	3050.628	77.62 %	G3-O4-4	2466.842	84.53 %
	G1-O4-5	4371.206	67.91 %	G2-O4-5	3636.479	92.53 %	G3-O4-5	2837.434	97.23 %
	G1-O4-6	4307.180	66.92 %	G2-O4-6	3745.517	95.30 %	G3-O4-6	2899.535	99.35 %
	G1-O4-7	4435.168	68.91 %	G2-O4-7	3087.385	78.56 %	G3-O4-7	2476.866	84.87 %
	G1-O4-8	4645.056	72.17 %	G2-O4-8	3293.902	83.81 %	G3-O4-8	2878.589	98.64 %
	G1-O4-9	4274.757	66.42 %	G2-O4-9	2929.312	74.54 %	G3-O4-9	2539.958	87.03 %
	G1-O4-10	3792.297	58.92 %	G2-O4-10	3055.501	77.75 %	G3-O4-10	2606.691	89.32 %
	G1-O4-11	3748.318	58.24 %	G2-O4-11	2860.928	72.80 %	G3-O4-11	2461.616	84.35 %
	G1-O4-12	3930.926	61.07 %	G2-O4-12	3471.954	88.34 %	G3-O4-12	2879.588	98.67 %
0.3H = 600	G1-O6-1	6433.725	99.96 %	G2-O6-1	3877.815	98.67 %	G3-O6-1	2910.077	99.72 %
	G1-O6-2	6367.764	98.93 %	G2-O6-2	3902.459	99.30 %	G3-O6-2	2915.291	99.89 %
	G1-O6-3	6426.344	99.84 %	G2-O6-3	3840.284	97.72 %	G3-O6-3	2823.924	96.76 %
	G1-O6-5	2932.362	45.56 %	G2-O6-4	2184.450	55.58 %	G3-O6-4	1905.263	65.29 %
	G1-O6-8	2750.217	42.73 %	G2-O6-5	2433.446	61.92 %	G3-O6-5	2281.666	78.18 %
	G1-O6-11	2181.485	33.89 %	G2-O6-6	2453.764	62.44 %	G3-O6-6	2321.569	79.55 %
				G2-O6-7	2364.532	60.17 %	G3-O6-7	2364.532	81.02 %
				G2-O6-8	2912.322	74.10 %	G3-O6-8	2912.322	99.79 %
				G2-O6-9	2186.385	55.63 %	G3-O6-9	1951.661	66.88 %
				G2-O6-10	2071.102	52.70 %	G3-O6-10	1863.150	63.84 %
				G2-O6-11	1992.830	50.71 %	G3-O6-11	1766.685	60.54 %
				G2-O6-12	2743.998	69.82 %	G3-O6-12	2784.150	95.40 %
0.4H = 800	G1-O8-1	6428.405	99.88 %	G2-O8-1	3900.265	99.24 %	G3-O8-1	2900.026	99.37 %
	G1-O8-2	6420.938	99.76 %	G2-O8-2	3910.312	99.50 %	G3-O8-2	2904.769	99.53 %
	G1-O8-3	6417.280	99.70 %	G2-O8-3	3864.244	98.33 %	G3-O8-3	2901.887	99.44 %
	G1-O8-5	2300.043	35.73 %	G2-O8-4	1558.595	39.66 %	G3-O8-4	1499.811	51.39 %
	G1-O8-8	2000.257	31.08 %	G2-O8-5	1550.257	39.45 %	G3-O8-5	1492.133	51.13 %
	G1-O8-11	1920.440	29.84 %	G2-O8-6	1657.056	42.16 %	G3-O8-6	1535.493	52.61 %
				G2-O8-7	1664.903	42.36 %	G3-O8-7	1459.040	50.00 %
				G2-O8-8	1800.043	45.80 %	G3-O8-8	1788.010	61.27 %
				G2-O8-9	1668.833	42.46 %	G3-O8-9	1494.240	51.20 %
				G2-O8-10	1464.481	37.26 %	G3-O8-10	1394.700	47.79 %
				G2-O8-11	1367.825	34.80 %	G3-O8-11	1233.700	42.27 %
				G2-O8-12	1576.519	40.11 %	G3-O8-12	1689.190	57.88 %

span deflection response, von Mises stress, tension and compression damage, and reinforcement yield for the studied beams. These data have been separately analyzed, categorized, and presented for each numerical series, as defined in the parametric study.

5.1. Effect of the opening on the ultimate load

5.1.1. Effect of the shear span-to-height ratio (a/H), opening size, and opening location

Series 1: for $f_c^{'} = 32\,\mathrm{N/mm^2}$

The 99 specimens in series 1 were analyzed to examine the effects of the shear span-to-height ratio (a/H), opening size, and opening location on the ultimate load. Series 1 specimens had identical material properties. Therefore, the effects of the compressive strength of concrete can be assumed to be uniform for the series-1 specimens.

Fig. 4 shows the relationship between the ultimate load ratio (P_{uo}/P_{us}%), which is the ratio of ultimate load for studied beams with openings compared to reference beams without openings, with the shear span-to-height ratio. Moreover, the results of the ultimate load and ultimate load ratio for the analyzed specimens are shown in Table 4. For specimens with identical conditions except for the opening size, location, and shear span-to-height ratio (a/H), increasing the shear span-to-height ratio (a/H) decreased the ultimate load of the studied beams. This reduction was insignificant for specimens with opening locations 1, 2, and 3 (openings through the flexural zone). Beams with opening locations through the loading path (locations 4, 9, and 11) or near the bearing plates (location 11) showed a more significant decrease in ultimate load.

Fig. 4 and Table 4 show that an increase in opening size decreases the ultimate load of the tested specimens. This effect is evident for specimens with an opening size of 800 mm due to the decrease in beam stiffness for a larger opening size, which intersects the loading trajectory between the loading plate and bearing plate. This setup can lead to higher stress concentrations and openings, which decreases the ultimate load.

Fig. 4 specimens with openings in the flexural zone (locations 1, 2, and 3) showed an insignificant influence of the openings on the capacity of beams and approached the ultimate load of reference beams without openings. Therefore, these locations do not affect the ultimate load of the reinforced concrete deep beams and are considered the best locations to make openings in deep beams.

Openings located through the shear zone cause a considerable decrease in the ultimate load of the examined deep beams, particularly openings through the load path (specimens: G1-O4-10, G1-O6-11, G1-O8-11, G2-O4-9, G2-O6-11, G2-O8-11, G3-O4-4, G3-O6-11, and G3-O8-11). This load path through the shear zone can also be defined as a critical path with the trajectory from the loading point to the bearing. Moreover, those specimens with openings near the bearing plates showed the lowest ultimate load and can be described as the worst locations (locations 4, 7, 9, 10, and 11 for specimens in Group 1, Group 2, and Group 3).

The results in Table 4 show that an increase in shear span-to-height ratio (a/H) for the same opening location significantly decreases the ultimate load. For example, for an opening size of 0.2H (400 mm), the ultimate loads for G1-O4-4, G2-O4-4, and G3-O4-4 were determined to be approximately 4296.265 kN, 3050.628 kN, and 2466.842 kN, respectively. Moreover, the ultimate loads for G1-O4-9 (4274.757 kN), G2-O4-9 (2929.312 kN), and G3-O4-9 (2539.958 kN) showed a similar

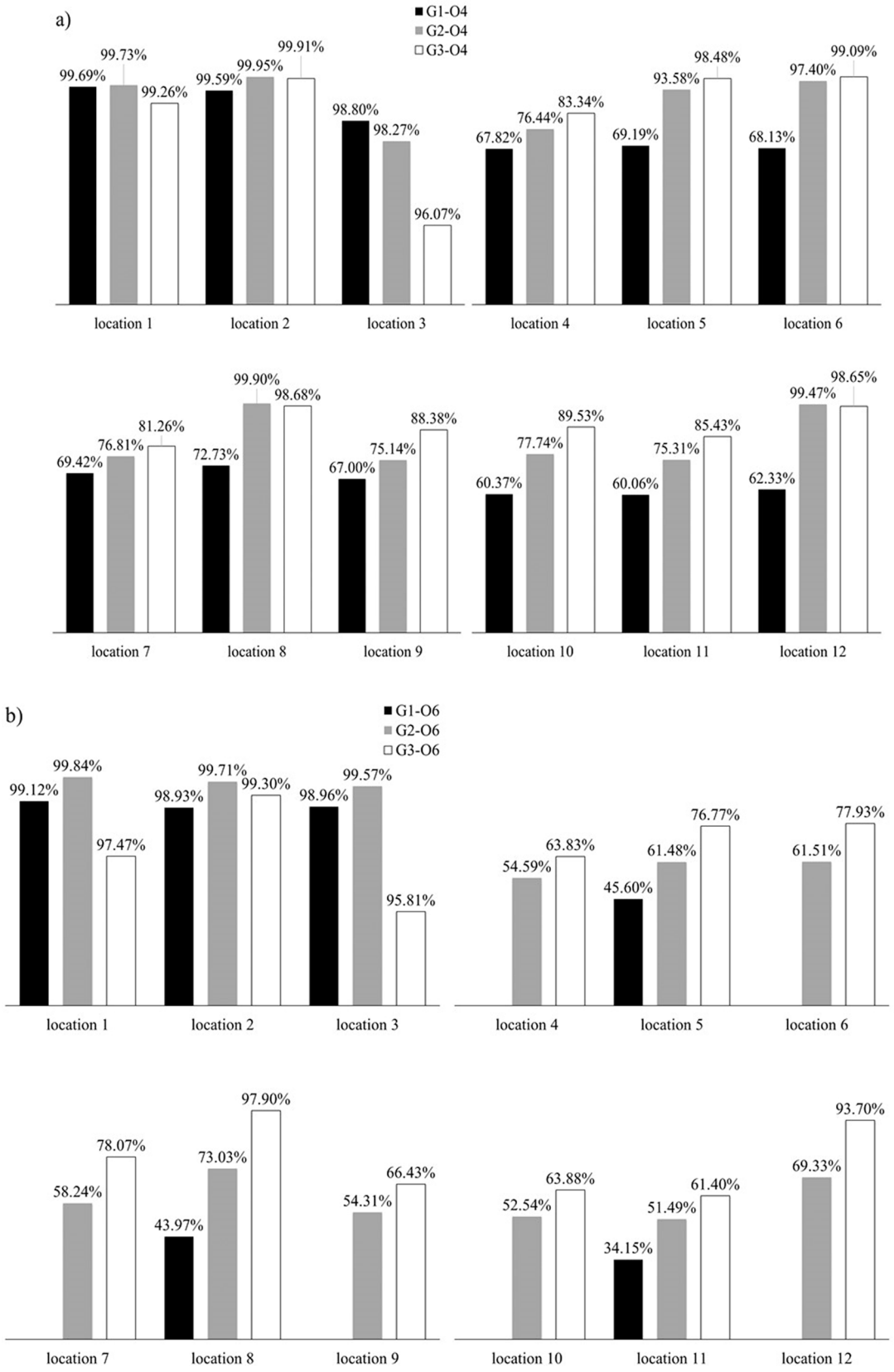

Fig. 5. Ultimate load of beams with openings to solid beam series 2. a). Beams with an opening size of 400 mm (0.2H – G1, G2, and G3). b). Beams with an opening size of 600 mm (0.3H– G1, G2, and G3). c). Beams with an opening size of 800 mm (0.4H– G1, G2, and G3). d). Beams with an opening size of 400 mm (0.2H– G4, G5, G6, G7, and G8).

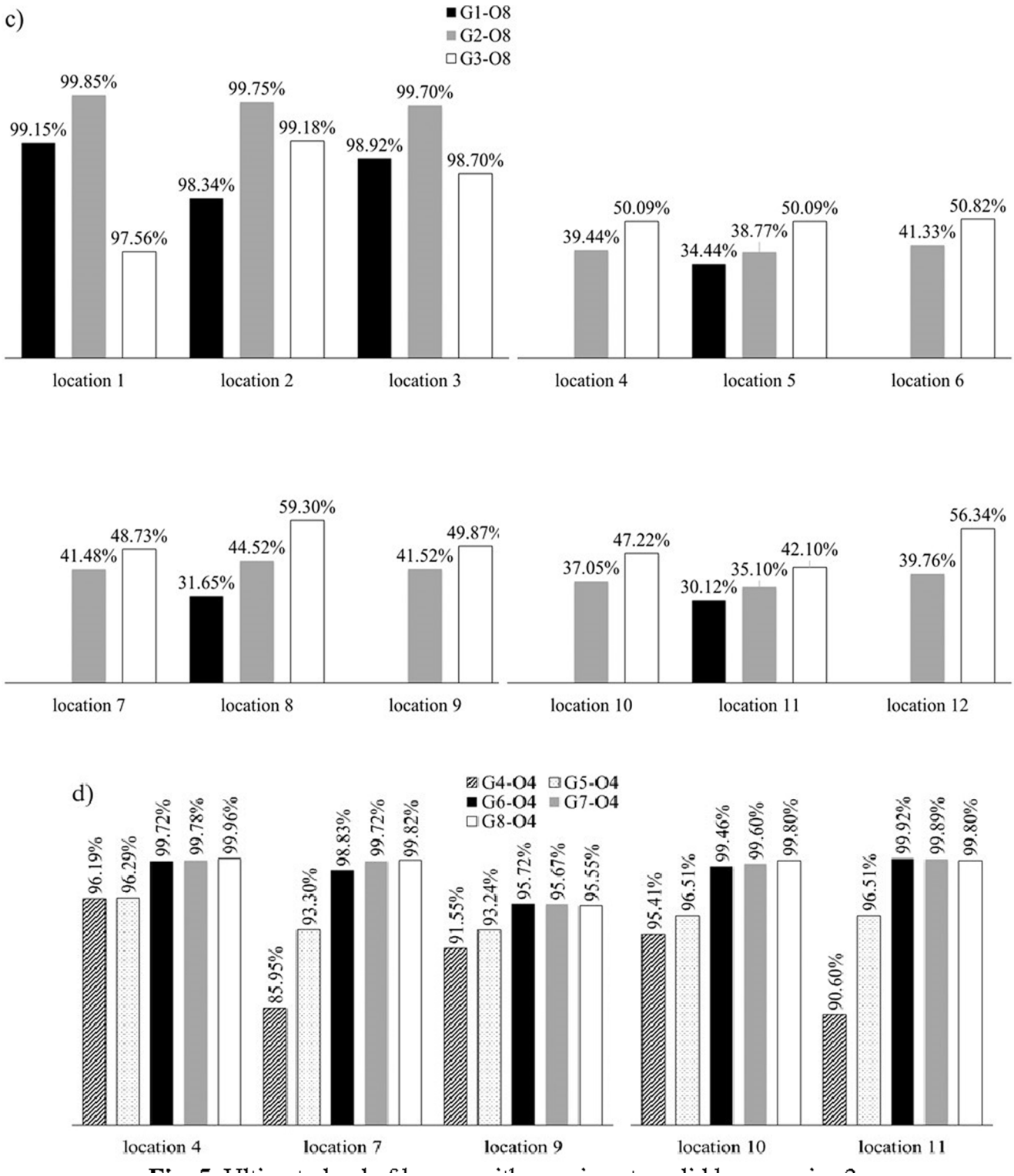

Fig. 5. (*continued*).

Table 5
Numerical results of the tested beams in series 2.

Group	G1($a/H = 0.25$)			G2 ($a/H = 0.5$)			G3 ($a/H = 0.75$)		
Opening size (mm)	Specimen Name	P_u(kN)	P_{uo}/P_{us}	specimen Name	P_u(kN)	P_{uo}/P_{us}	specimen Name	P_u(kN)	P_{uo}/P_{us}
zero	G1-Ozero	7328.65	100 %	G2-Ozero	4479.509	100 %	G3-Ozero	3340.158	100 %
0.2H = 400	G1-O4-1	7325.804	99.96 %	G2-O4-1	4404.502	98.33 %	G3-O4-1	3292.51	98.57 %
	G1-O4-2	7298.483	99.59 %	G2-O4-2	4470.374	99.80 %	G3-O4-2	3330.374	99.71 %
	G1-O4-3	7321.076	99.90 %	G2-O4-3	4455.879	99.47 %	G3-O4-3	3180.606	95.22 %
	G1-O4-4	4998.73	68.21 %	G2-O4-4	3370.597	75.24 %	G3-O4-4	2755.395	82.49 %
	G1-O4-5	5108.111	69.70 %	G2-O4-5	4191.882	93.58 %	G3-O4-5	3254.417	97.43 %
	G1-O4-6	5029.151	68.62 %	G2-O4-6	4403.035	98.29 %	G3-O4-6	3247.551	97.23 %
	G1-O4-7	5075.404	69.25 %	G2-O4-7	3367.846	75.18 %	G3-O4-7	2646.808	79.24 %
	G1-O4-8	5322.865	72.63 %	G2-O4-8	4407.02	98.38 %	G3-O4-8	3219.318	96.38 %
	G1-O4-9	4900.242	66.86 %	G2-O4-9	3393.948	75.77 %	G3-O4-9	2954.561	88.46 %
	G1-O4-10	4480.65	61.14 %	G2-O4-10	3477.516	77.63 %	G3-O4-10	3000.988	89.85 %
	G1-O4-11	4476.139	61.08 %	G2-O4-11	3417.249	76.29 %	G3-O4-11	2857.728	85.56 %
	G1-O4-12	4619.492	63.03 %	G2-O4-12	4133.782	92.28 %	G3-O4-12	3320.181	99.40 %
0.3H = 600	G1-O6-1	7327.477	99.98 %	G2-O6-1	4403.275	98.30 %	G3-O6-1	3331.279	99.73 %
	G1-O6-2	7253.704	98.98 %	G2-O6-2	4421.316	98.70 %	G3-O6-2	3338.923	99.96 %
	G1-O6-3	7324.198	99.94 %	G2-O6-3	4398.505	98.19 %	G3-O6-3	3183.582	95.31 %
	G1-O6-5	3315.584	45.24 %	G2-O6-4	2410.036	53.80 %	G3-O6-4	2102.731	62.95 %
	G1-O6-8	3245.005	44.28 %	G2-O6-5	2709.539	60.49 %	G3-O6-5	2516.322	75.34 %
	G1-O6-11	2491.763	34.00 %	G2-O6-6	2709.922	60.50 %	G3-O6-6	2557.101	76.56 %
				G2-O6-7	2540.04	56.70 %	G3-O6-7	2046.568	61.27 %
				G2-O6-8	3204.012	71.53 %	G3-O6-8	3035.535	90.88 %
				G2-O6-9	2386.097	53.27 %	G3-O6-9	2203.699	65.98 %
				G2-O6-10	2345.162	52.35 %	G3-O6-10	2150.32	64.38 %
				G2-O6-11	2300.805	51.36 %	G3-O6-11	2049.777	61.37 %
				G2-O6-12	3070.349	68.54 %	G3-O6-12	3073.802	92.03 %
0.4H = 800	G1-O8-1	7321.419	99.90 %	G2-O8-1	4417.907	98.62 %	G3-O8-1	3316.296	99.29 %
	G1-O8-2	7215.961	98.46 %	G2-O8-2	4446.159	99.26 %	G3-O8-2	3328.822	99.66 %
	G1-O8-3	7320.423	99.89 %	G2-O8-3	4412.611	98.51 %	G3-O8-3	3282.924	98.29 %
	G1-O8-5	2493.496	34.02 %	G2-O8-4	1745.2	38.96 %	G3-O8-4	1643.867	49.22 %
	G1-O8-8	2309.326	31.51 %	G2-O8-5	1709.326	38.16 %	G3-O8-5	1644.083	49.22 %
	G1-O8-11	2197.99	29.99 %	G2-O8-6	1820.042	40.63 %	G3-O8-6	1667.061	49.91 %
				G2-O8-7	1825.438	40.75 %	G3-O8-7	1593.212	47.70 %
				G2-O8-8	1943.496	43.39 %	G3-O8-8	1929.344	57.76 %
				G2-O8-9	1834.325	40.95 %	G3-O8-9	1628.854	48.77 %
				G2-O8-10	1645.378	36.73 %	G3-O8-10	1570.732	47.03 %
				G2-O8-11	1551.81	34.64 %	G3-O8-11	1392.245	41.68 %
				G2-O8-12	1761.634	39.33 %	G3-O8-12	1879.525	56.27 %

trend. Likewise, the ultimate loads for G1-O4-11 (3748.318 kN), G2-O4-11 (2860.928 kN), and G3-O4-11 (2461.616 kN) were reduced with an increase in shear span-to-height ratio (a/H). The ultimate loads of RC deep beams with 0.3H (600 mm) and 0.4H (800 mm) web opening sizes also demonstrated similar behavior. For the 0.3H web opening size, the ultimate load values for G1-O6-11, G2-O6-11, and G3-O6-11 were 2181.485 kN, 1992.830 kN, and 1766.685 kN, respectively; for the 0.4H (800 mm) web opening size, the ultimate load for G1-O8-11, G2-O8-11, and G3-O8-11 was 1920.440 kN, 1367.825 kN, and 1233.700 kN, respectively. Consequently, the observed ultimate load ratio (P_{uo}/P_{us}%) improved with the increase in shear span-to-height ratio (a/H) for all opening sizes. The reason behind this finding is that the web opening has a lesser effect on the ultimate load ratio (P_{uo}/P_{us}%) for a greater shear span-to-height ratio (a/H) = 0.75. The specimens with a smaller shear span-to-height ratio (a/H) = 0.25 showed a lower ultimate load ratio due to the significant effect of the web opening on decreasing the capacity of the RC deep beams. Table 4 shows that for an opening size of 0.2H (400 mm) and a shear span-to-height ratio (a/H) of 0.25, 0.5, and 0.75, the ultimate load ratios (P_{uo}/P_{us}%) for G1-O4-4, G2-O4-4, and G3-O4-4 are 66.75 %, 77.62 %, and 84.53 %, respectively. For a 0.3H (600 mm) opening size and a shear span-to-height ratio (a/H) of 0.25, 0.5, and 0.75, the ultimate load ratios (P_{uo}/P_{us}%) for G1-O6-11, G2-O6-11, and G3-O6-11 are 33.89 %, 50.71 %, and 60.54 %, respectively. Moreover, for a 0.4H (800 mm) opening size and a shear span-to-height ratio (a/H) of 0.25, 0.5, and 0.75, the ultimate load ratios (P_{uo}/P_{us}%) for G1-O8-11, G2-O8-11, and G3-O8-11 were determined to be 29.84 %, 34.80 %, and 42.27 %, respectively. These analyzed results confirm the improvement of the ultimate load ratio of beams with openings in comparison with the beams without openings (P_{uo}/P_{us}%). The reason is that the opening, in this case, intersects the load path between the loading plate and bearing plate, which results in a more significant decrease in ultimate load compared to the cases of beams with a greater shear span-to-height ratio ($a/H = 0.75$).

Series 2 for $f_c^{'} = 40\,\mathrm{N/mm^2}$

The 129 specimens in series 2 were analyzed to examine the effects of the shear span-to-height ratio (a/H), opening size, and opening location when using a higher concrete strength with $f_c^{'} = 40\,\mathrm{N/mm^2}$. Series-2 specimens had identical material properties. Therefore, similar to series 1, the effects of the compressive strength of concrete can be assumed to be uniform for the series-2 specimens.

The relationship between the ultimate load ratio (P_{uo}/P_{us}%) and the shear span-to-height ratio is presented in Fig. 5. All ultimate load and ultimate load ratio results for the tested specimens in series 2 are presented in Table 5. A greater increase in shear span-to-height ratio (a/H) corresponds to a lower ultimate load. This reduction was insignificant for specimens with opening locations 1, 2, and 3 (openings through the flexural zone). However, opening locations through the load path (locations 4, 9, and 11) showed a more considerable reduction in the ultimate load.

Fig. 5 and Table 5 show that increasing the opening size for the tested beams decreased the ultimate load for the tested beams, especially for specimens with an opening size of 800 mm, because the highest stress concentration was at the opening corners. These corners were considered the nodes that joined the loading path from the loading point to the support point, as shown in Fig. 7 (c). The internal stress concentration at a weak point of the beam reduced the ultimate capacity of the beam. Fig. 7 (a), (b), and (d) show that the concrete area below the opening and near the support was exposed to biaxial stresses (tension and

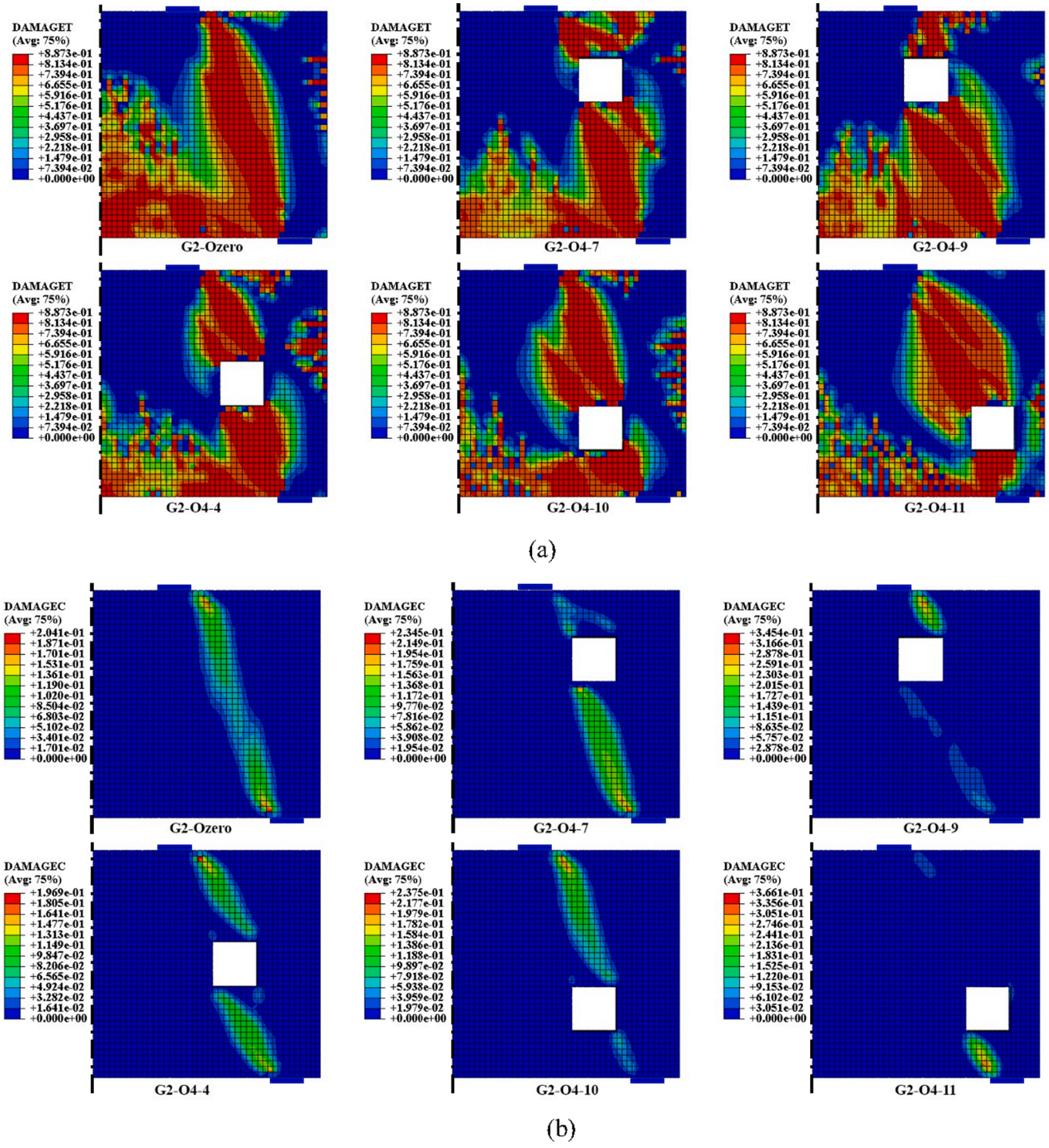

Fig. 6. Effect of the opening location. a) Damage in tension. b) Damage in compression. c) von Mises for concrete deep beams. d) Tensile stresses for the web and main reinforcement.

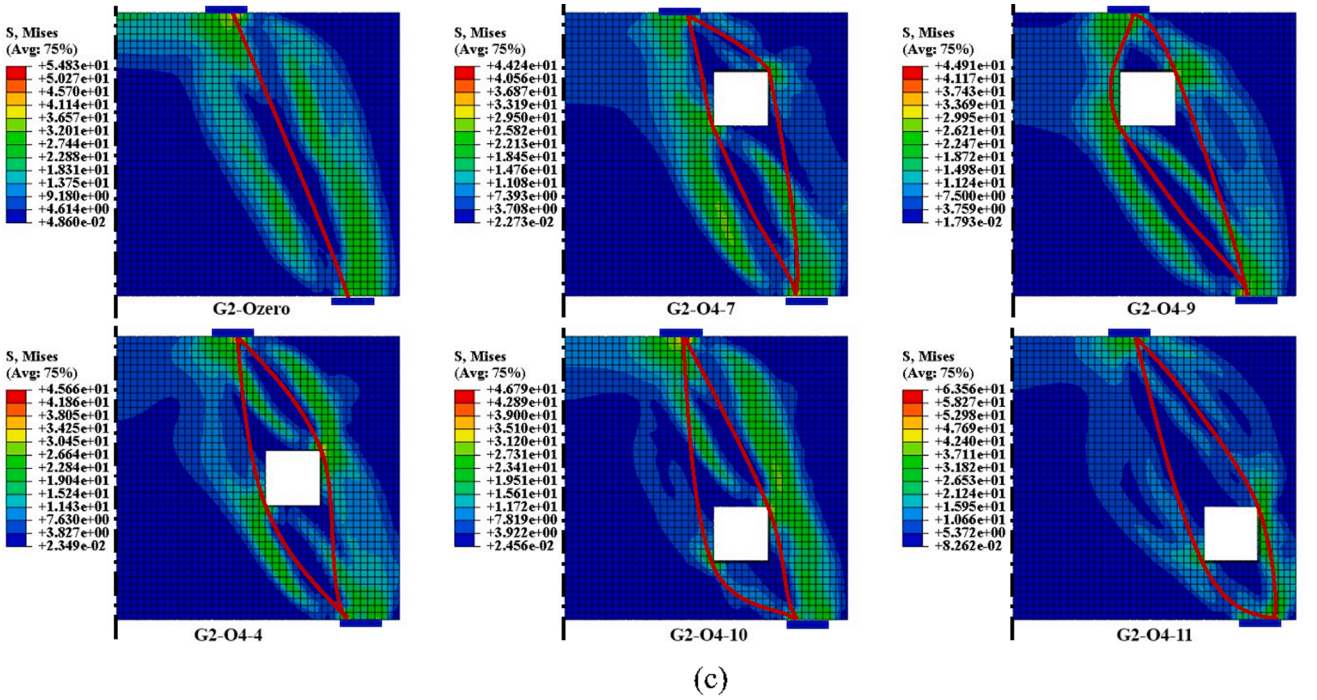

(c)

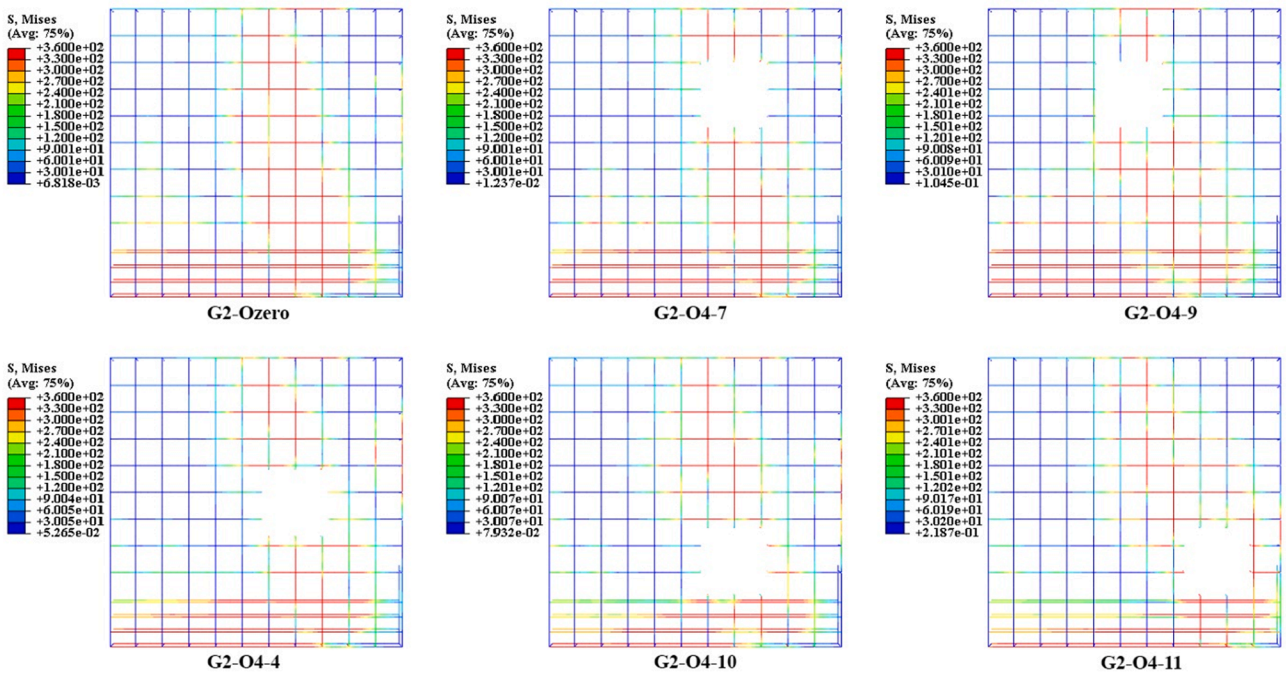

(d)

Fig. 6. (*continued*).

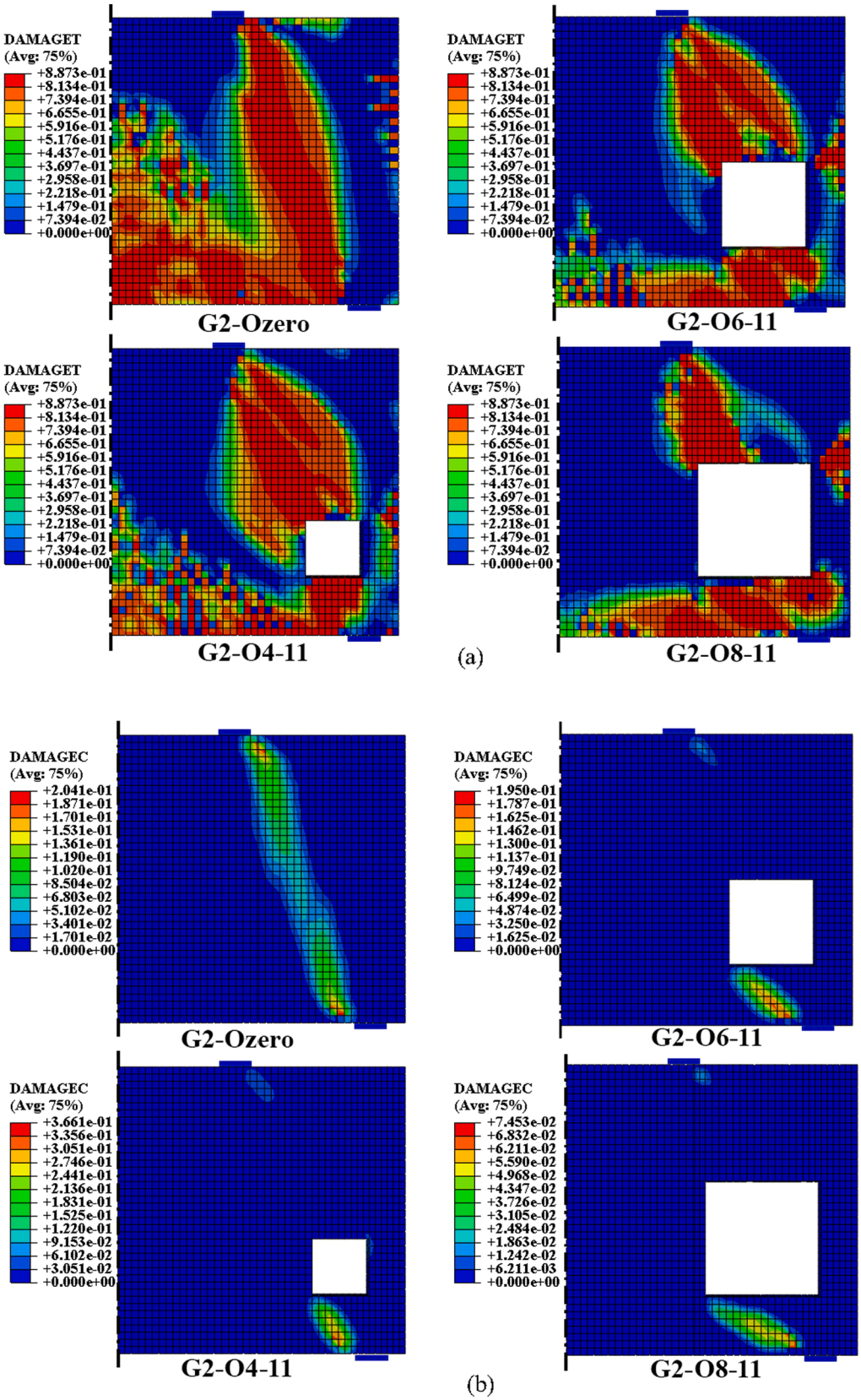

Fig. 7. Effect of the opening size. a) Damage in tension. b) Damage in compression. c) von Mises for concrete deep beams. d) Tensile stresses for the web and main reinforcement.

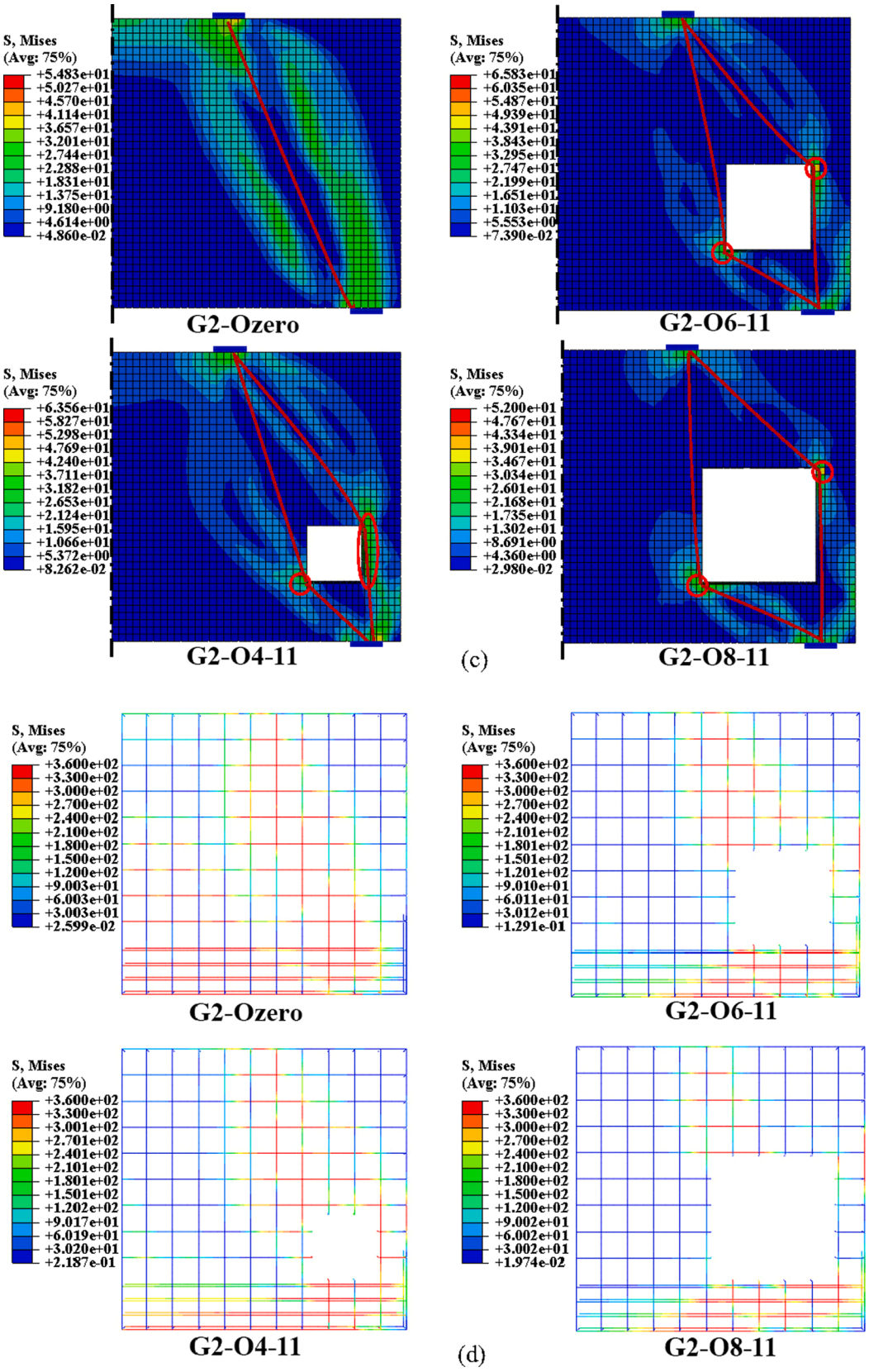

Fig. 7. (*continued*).

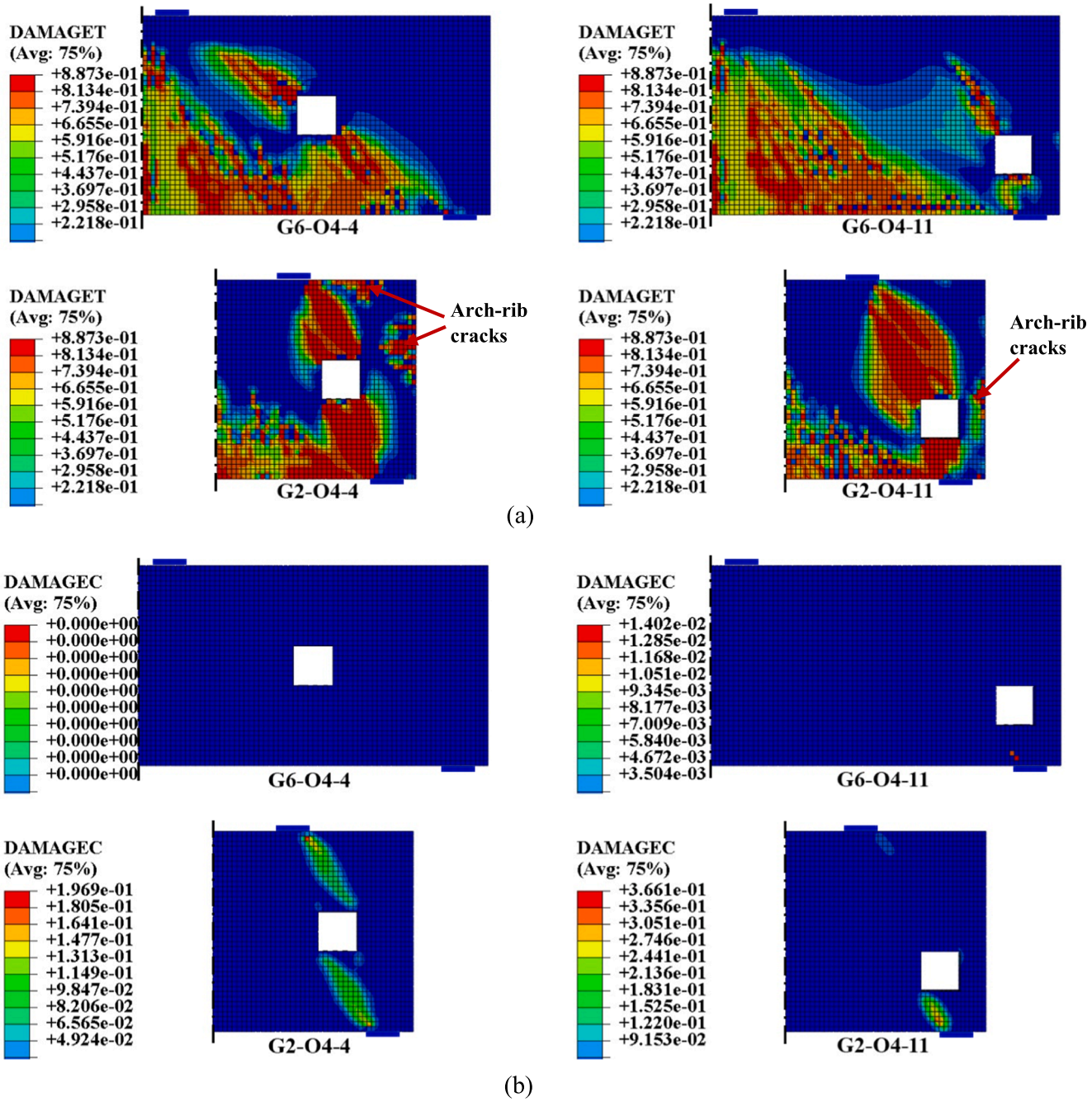

Fig. 8. Effect of the shear span-to-height ratio (*a/H*). a) Damage in tension. b) Damage in compression. c) von Mises for concrete deep beams. d) Tensile stresses for the web and main reinforcement.

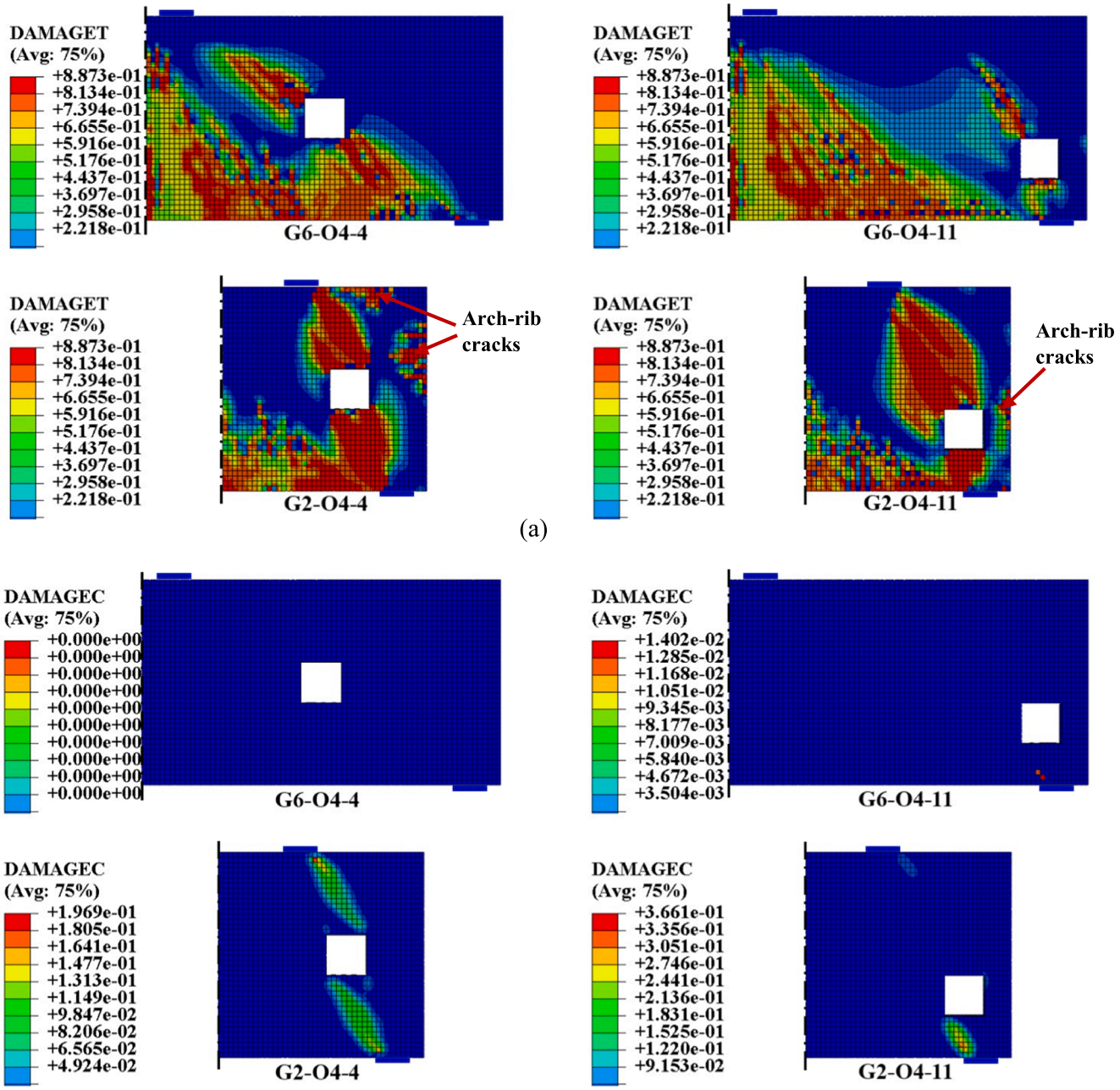

Fig. 8. (*continued*).

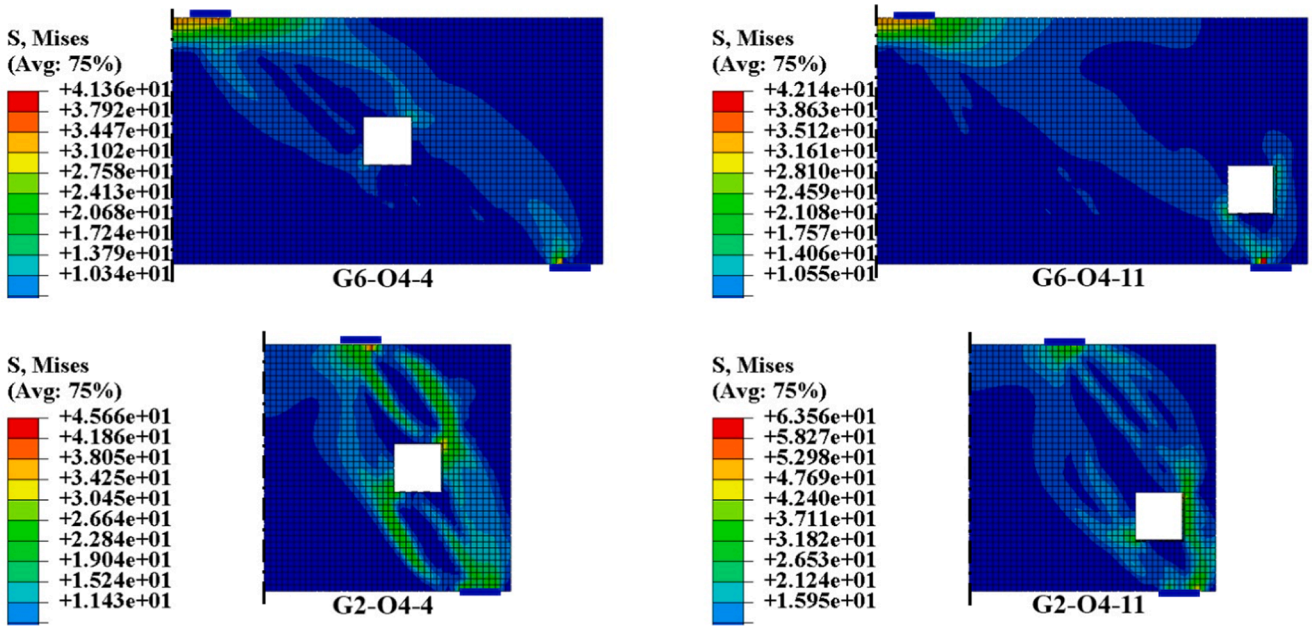

(c)

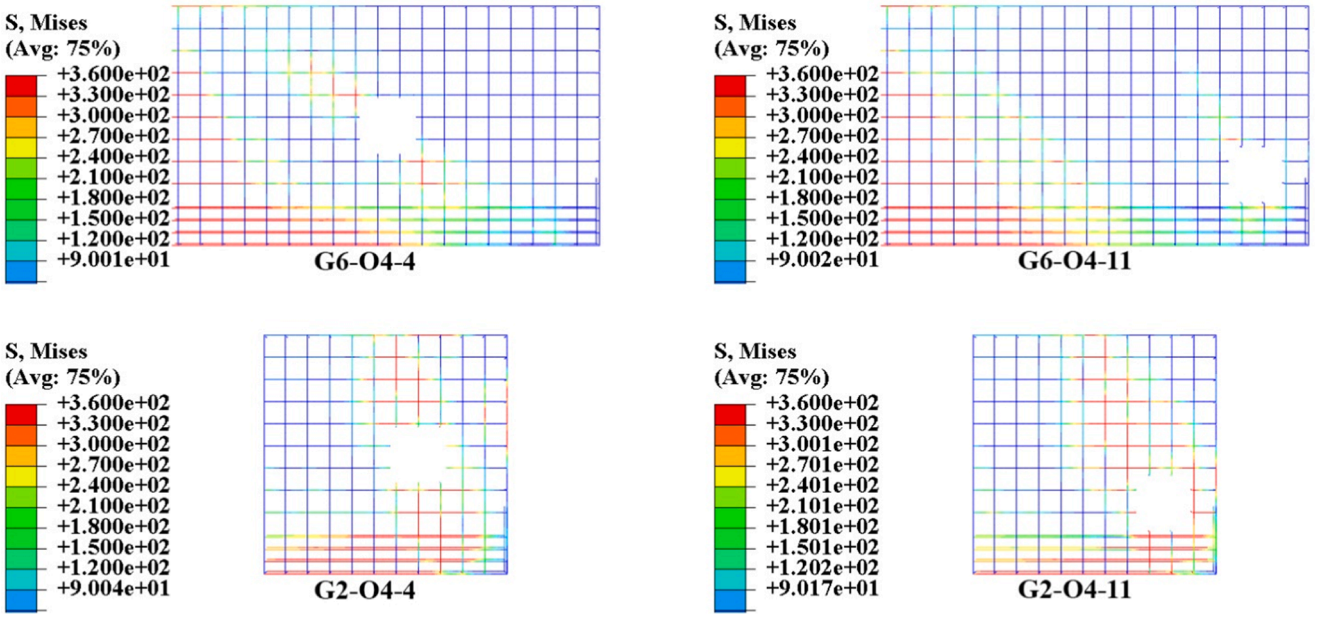

(d)

Fig. 8. (*continued*).

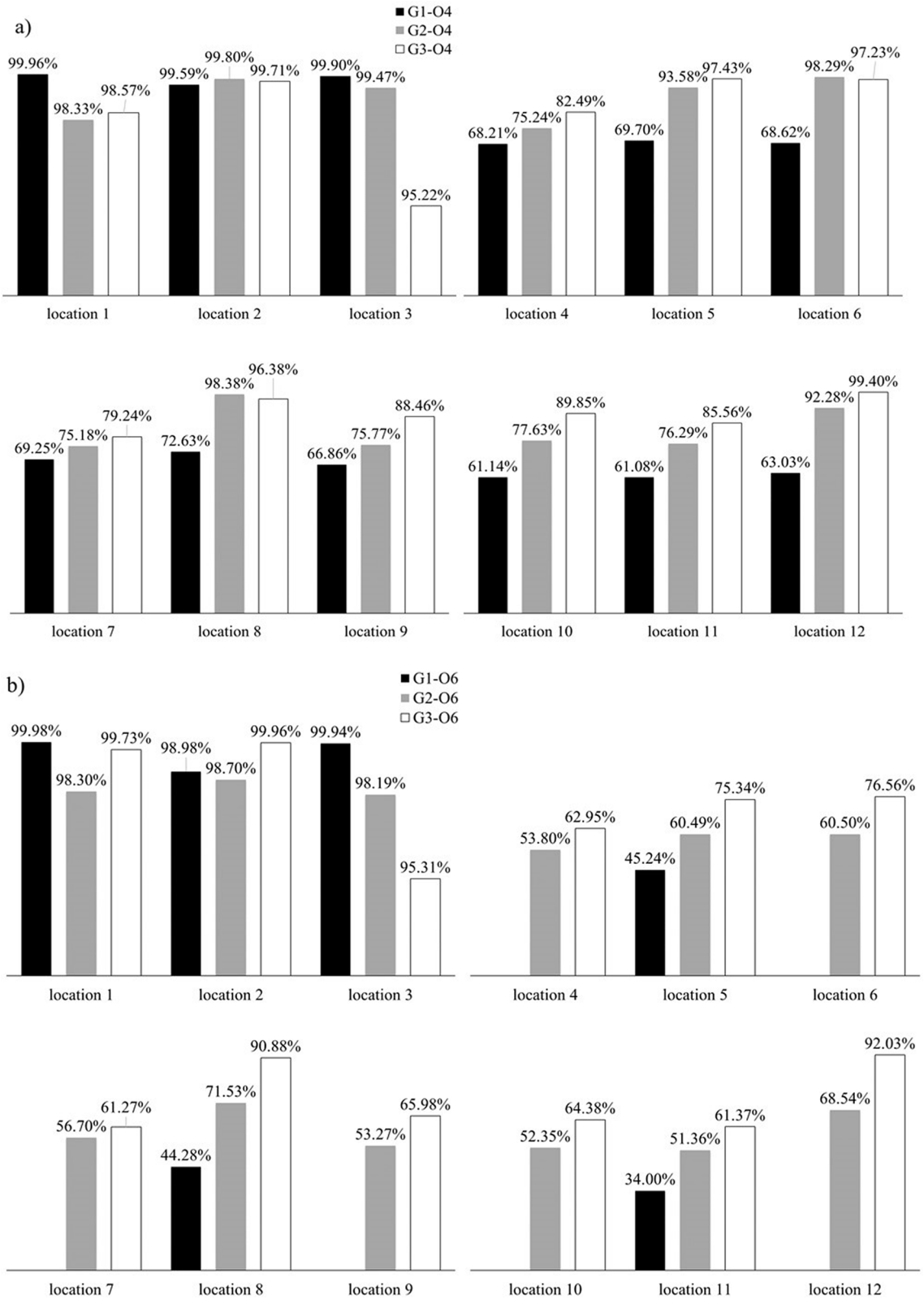

Fig. 9. Ultimate load of beams with openings to solid beam series 3.a). Beams with an opening size of 400 mm (0.2H). b). Beams with openings of 600 mm (0.3H). c). Beams with openings of 800 mm (0.4H).

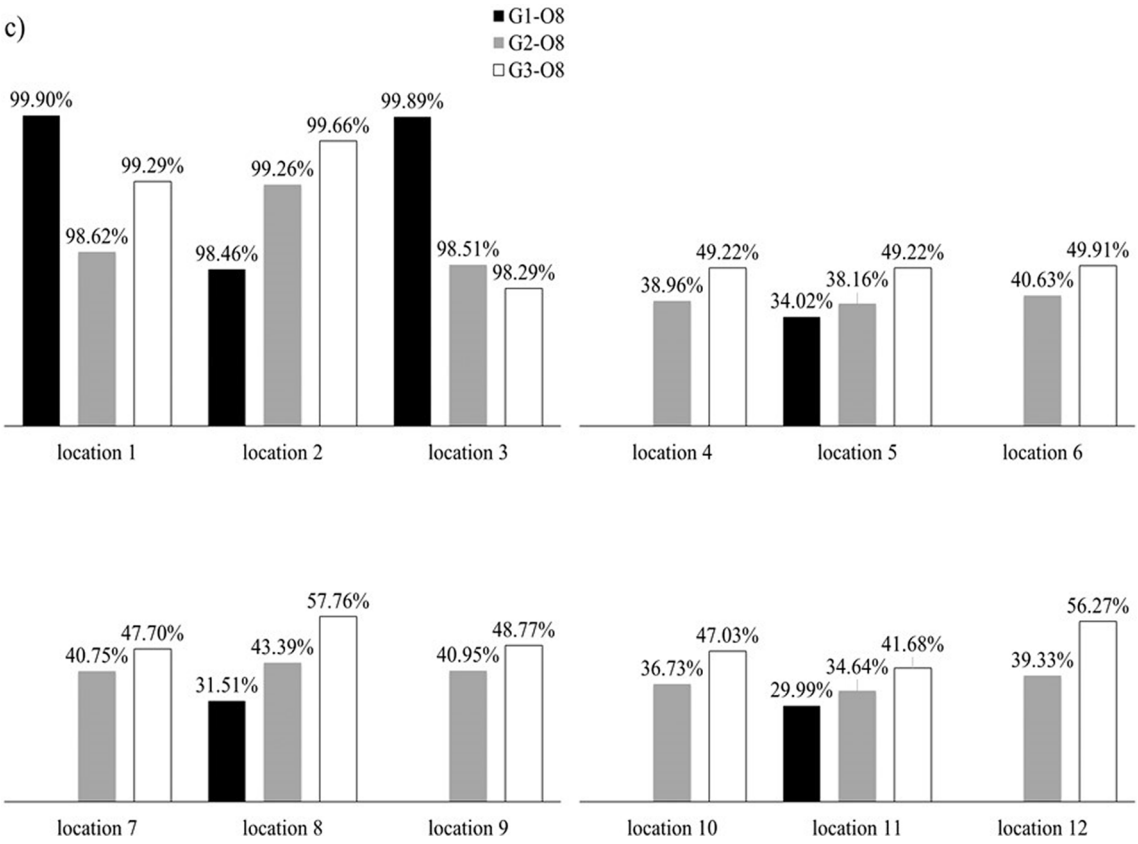

Fig. 9. (*continued*).

compression stresses), which decreased the concrete load resistance; hence, the steel reinforcement was responsible for resisting shear stresses.

Fig. 5 shows that openings in the flexural zone (locations 1, 2, and 3) had almost no effect on the ultimate load of the reinforced concrete deep beams and were considered the best locations for making openings in deep beams. However, a significant reduction was noticed in the ultimate load of the tested beams with openings through the load path (specimens: G1-O4-10, G1-O6-11, G1-O8-11, G2-O4-9, G2-O6-11, G2-O8-11, G3-O4-4, G3-O6-11, and G3-O8-11). The worst locations were 4, 7, 9, 10, and 11 for specimens in Group 1, Group 2, and Group 3. The damage in tension and compression, von Mises stress, and tensile stress of steel reinforcement are presented in Fig. 6 for the worst opening locations in Group 2. The loading path splits into two paths, the upper and lower, represented by the red lines in Fig. 6 (c).

According to Table 5 results, for all studied cases of web opening sizes (0.2H, 0.3H, and 0.4H), the observed ultimate load decreased with the increase in shear span-to-height ratio (a/H) for beams with identical opening locations. For instance, for an opening size of 0.2H (400 mm), the ultimate loads for G1-O4-4, G2-O4-4, and G3-O4-4 were 4677.448 kN, 3219.946 kN, and 2618.740 kN, respectively. Similarly, the ultimate loads for G1-O4-11, G2-O4-11, and G3-O4-11 were approximately 4141.9 kN, 3172.2 kN, and 2684.6 kN, respectively. In addition, for opening sizes of 0.3H (600 mm) and 0.4H (800 mm), a similar behavior was observed. For the 0.3H (600 mm) opening size, the ultimate loads for the G1-O6-11, G2-O6-11, and G3-O6-11 beams were 2355.429 kN, 2168.774 kN, and 1929.364 kN, respectively. Furthermore, for a 0.4H (800-mm) opening size, the ultimate loads for G1-O8-11, G2-O8-11, and G3-O8-11 were approximately 2077.510 kN, 1478.664 kN, and 1322.864 kN, respectively. Additionally, due to the minor effect of the web opening on the ultimate load ratio (P_{uo}/P_{us}%) for a higher shear span-to-height ratio (a/H), the observed ultimate load ratio (P_{uo}/P_{us}%) improved with the increase in shear span-to-height ratio (a/H) for all opening sizes. The specimens with a smaller shear span-to-height ratio (a/H), such as 0.25, noticed a significant reduction in ultimate load due to the higher effect of the web opening on the capacity of the RC deep beams. Table 5 shows that for 0.2H (400-mm) opening sizes and shear span-to-height ratios (a/H) of 0.25, 0.5, and 0.75, the ultimate load ratios (P_{uo}/P_{us}%) for G1-O4-4, G2-O4-4, and G3-O4-4 were approximately 67.82 %, 76.44 %, and 83.34 %, respectively. A similar increase in ultimate load ratios (P_{uo}/P_{us}%) is clearly shown in Table 5 for beam specimens with 0.2H (400 mm), 0.3H (600 mm), and 0.4H (800 mm) opening sizes. These results confirm the improvement in the ratio of the ultimate load of beams with openings to that without openings (P_{uo}/P_{us}%). The reason is that the opening, in this case, intersects the load path between the loading plate and the bearing plate, which results in a greater drop in the ultimate load compared to the cases of beams with a greater shear span-to-height ratio ($a/H = 0.75$).

An additional five groups were analyzed with larger shear span-to-depth ratios of 1, 1.25, 1.5, 1.75, and 2 for G4, G5, G6, G7, and G8, respectively. The analysis results for the examined groups confirmed the findings of the other three groups: increasing the (a/H) ratio enhances the ultimate load ratio (P_{uo}/P_{us}%). Therefore, the existence of openings through the strut that joins the loading point and supporting point had a negligible effect on the reduction of (P_{uo}) due to the flexural effect for beams with higher values of (a/H). Since the examined specimens had longer shear spans, some or part of the internal stresses moved to the supporting point through the main reinforcement. Additionally, the longer shear span allows the internal forces to transfer around the opening, joining the strut between the loading and supporting points. The crack propagation at the beams and distribution of stresses along the reinforcement steel bars, which are presented in Fig. 8, confirmed this explanation.

Series 3 for $f_c^{'} = 48\,\mathrm{N/mm^2}$

The 99 specimens in series 3 were analyzed to examine the effects of the shear span-to-height ratio (a/H), opening size, and opening location

Table 6
Numerical results of the tested beams in series 3.

Group	G1($a/H = 0.25$)			G2 ($a/H = 0.5$)			G3 ($a/H = 0.75$)		
Opening size (mm)	Specimen Name	P_u(kN)	P_{uo}/P_{us}	specimen Name	P_u(kN)	P_{uo}/P_{us}	specimen Name	P_u(kN)	P_{uo}/P_{us}
zero	G1-Ozero	6896.355	100 %	G2-Ozero	4212.348	100 %	G3-Ozero	3142.356	100 %
0.2H = 400	G1-O4-1	6875.088	99.69 %	G2-O4-1	4200.856	99.73 %	G3-O4-1	3119.198	99.26 %
	G1-O4-2	6867.892	99.59 %	G2-O4-2	4210.422	99.95 %	G3-O4-2	3139.422	99.91 %
	G1-O4-3	6813.920	98.80 %	G2-O4-3	4139.666	98.27 %	G3-O4-3	3018.717	96.07 %
	G1-O4-4	4677.448	67.82 %	G2-O4-4	3219.946	76.44 %	G3-O4-4	2618.740	83.34 %
	G1-O4-5	4771.650	69.19 %	G2-O4-5	3941.904	93.58 %	G3-O4-5	3094.491	98.48 %
	G1-O4-6	4698.317	68.13 %	G2-O4-6	4102.914	97.40 %	G3-O4-6	3113.679	99.09 %
	G1-O4-7	4787.542	69.42 %	G2-O4-7	3235.392	76.81 %	G3-O4-7	2553.342	81.26 %
	G1-O4-8	5015.733	72.73 %	G2-O4-8	4208.214	99.90 %	G3-O4-8	3101.031	98.68 %
	G1-O4-9	4620.863	67.00 %	G2-O4-9	3165.237	75.14 %	G3-O4-9	2777.143	88.38 %
	G1-O4-10	4163.353	60.37 %	G2-O4-10	3274.870	77.74 %	G3-O4-10	2813.227	89.53 %
	G1-O4-11	4141.861	60.06 %	G2-O4-11	3172.207	75.31 %	G3-O4-11	2684.633	85.43 %
	G1-O4-12	4298.210	62.33 %	G2-O4-12	4190.031	99.47 %	G3-O4-12	3099.936	98.65 %
0.3H = 600	G1-O6-1	6835.437	99.12 %	G2-O6-1	4205.550	99.84 %	G3-O6-1	3062.760	97.47 %
	G1-O6-2	6822.822	98.93 %	G2-O6-2	4200.012	99.71 %	G3-O6-2	3120.463	99.30 %
	G1-O6-3	6824.312	98.96 %	G2-O6-3	4194.272	99.57 %	G3-O6-3	3010.767	95.81 %
	G1-O6-5	3145.066	45.60 %	G2-O6-4	2299.628	54.59 %	G3-O6-4	2005.686	63.83 %
	G1-O6-8	3032.651	43.97 %	G2-O6-5	2589.687	61.48 %	G3-O6-5	2412.503	76.77 %
	G1-O6-11	2355.429	34.15 %	G2-O6-6	2591.166	61.51 %	G3-O6-6	2448.820	77.93 %
				G2-O6-7	2453.161	58.24 %	G3-O6-7	2453.161	78.07 %
				G2-O6-8	3076.286	73.03 %	G3-O6-8	3076.286	97.90 %
				G2-O6-9	2287.668	54.31 %	G3-O6-9	2087.391	66.43 %
				G2-O6-10	2212.976	52.54 %	G3-O6-10	2007.242	63.88 %
				G2-O6-11	2168.774	51.49 %	G3-O6-11	1929.364	61.40 %
				G2-O6-12	2920.217	69.33 %	G3-O6-12	2944.505	93.70 %
0.4H = 800	G1-O8-1	6837.714	99.15 %	G2-O8-1	4206.224	99.85 %	G3-O8-1	3065.702	97.56 %
	G1-O8-2	6781.733	98.34 %	G2-O8-2	4201.661	99.75 %	G3-O8-2	3116.561	99.18 %
	G1-O8-3	6821.931	98.92 %	G2-O8-3	4199.800	99.70 %	G3-O8-3	3101.494	98.70 %
	G1-O8-5	2375.241	34.44 %	G2-O8-4	1661.376	39.44 %	G3-O8-4	1574.127	50.09 %
	G1-O8-8	2182.965	31.65 %	G2-O8-5	1632.965	38.77 %	G3-O8-5	1574.073	50.09 %
	G1-O8-11	2077.510	30.12 %	G2-O8-6	1740.825	41.33 %	G3-O8-6	1597.085	50.82 %
				G2-O8-7	1747.365	41.48 %	G3-O8-7	1531.359	48.73 %
				G2-O8-8	1875.241	44.52 %	G3-O8-8	1863.398	59.30 %
				G2-O8-9	1748.927	41.52 %	G3-O8-9	1566.941	49.87 %
				G2-O8-10	1560.635	37.05 %	G3-O8-10	1483.827	47.22 %
				G2-O8-11	1478.664	35.10 %	G3-O8-11	1322.864	42.10 %
				G2-O8-12	1674.816	39.76 %	G3-O8-12	1770.251	56.34 %
Group	G4($a/H = 1$)			G5 ($a/H = 1.25$)			G6 ($a/H = 1.5$)		
zero	G4-Ozero	2557.350	100 %	G5-Ozero	2067.500	100 %	G6-Ozero	1666.330	100 %
0.2H = 400	G4-O4-4	2459.956	96.19 %	G5-O4-4	1990.711	96.29 %	G6-O4-4	1661.589	99.72 %
	G4-O4-7	2198.109	85.95 %	G5-O4-7	1928.952	93.30 %	G6-O4-7	1646.837	98.83 %
	G4-O4-9	2341.291	91.55 %	G5-O4-9	1927.693	93.24 %	G6-O4-9	1595.066	95.72 %
	G4-O4-10	2439.863	95.41 %	G5-O4-10	1995.426	96.51 %	G6-O4-10	1657.258	99.46 %
	G4-O4-11	2316.874	90.60 %	G5-O4-11	1995.426	96.51 %	G6-O4-11	1665.020	99.92 %
Group	G7($a/H = 1.75$)			G8 ($a/H = 2$)					
zero	G7-Ozero	1400.810	100 %	G8-Ozero	561.383	100 %			
	G7-O4-4	1397.747	99.78 %	G8-O4-4	561.164	99.96 %			
	G7-O4-7	1396.886	99.72 %	G8-O4-7	560.363	99.82 %			
	G7-O4-9	1340.114	95.67 %	G8-O4-9	536.393	95.55 %			
	G7-O4-10	1395.262	99.60 %	G8-O4-10	560.236	99.80 %			
	G7-O4-11	1399.318	99.89 %	G8-O4-11	560.253	99.80 %			

P_u: ultimate load.
P_{us}/P_{uo}: ratio of the ultimate load for the studied beams with openings compared to the reference beam without openings.

(similar to series 1 and 2) when using a higher concrete strength with $f_c^{'} = 48\,\mathrm{N/mm^2}$. Series-3 specimens had identical material properties, similar to series 1 and 2. Therefore, the effects of the compressive strength of concrete can be assumed to be uniform for the series-3 specimens.

Fig. 9 describes the relationship between the ultimate load ratio (P_{uo}/P_{us}%) and shear span-to-height ratio. The ultimate loads for the analyzed beams are shown in Table 6. Like series-1 and -2 results, series-3 results prove that increasing the shear span-to-height ratio (a/H) decreases the ultimate load of the studied beams. Fig. 9 and Table 6 show that the greater opening size for the tested specimens leads to a smaller ultimate load of the beam. This effect is significant for specimens with an opening size of 800 mm. Fig. 9 shows a negligible effect of the opening on the capacity of beams for the specimens with openings in the flexural zone (locations 1, 2, and 3). Therefore, these locations do not affect the ultimate load of the reinforced concrete deep beams and are considered the best locations for making openings in deep beams.

Specimens with openings through the shear zone showed a massive reduction in ultimate load, particularly if those openings were located through the load path. Specimens with opening locations 4, 7, 9, 10, and 11 in all studied groups showed the lowest ultimate load and could be described as the worst locations.

Table 6 shows that the ultimate load decreases with increasing shear span-to-height ratio (a/H) for the same opening location. For an opening size of 0.2H (400 mm), the ultimate loads for G1-O4-4, G2-O4-4, and G3-O4-4 were analyzed to be 4998.730 kN, 3370.597 kN, and 2755.395 kN, respectively. For an opening size of 0.3H (600 mm), the ultimate loads for G1-O6-11, G2-O6-11, and G3-O6-11 were 2491.763 kN, 2300.805

Table 7
Numerical results of the tested beams in series 4 and 5.

		Location 4 P_u(kN)	Reduction of ultimate load	Location 7 P_u(kN)	Reduction of ultimate load	Location 9 P_u(kN)	Reduction of ultimate load	Location 10 P_u(kN)	Reduction of ultimate load	Location 11 P_u(kN)	Reduction of ultimate load
Percent of ultimate load of specimens with varied ρ_s to the ultimate load of the beam without openings											
	Ozero	4212.348		4212.348		4212.348		4212.348		4212.348	
Effect of main reinforcement ratio (ρ_s)	0.21 %	2633.922	37.47 %	2557.826	39.28 %	2718.204	35.47 %	2833.107	32.74 %	2651.538	37.05 %
	0.25 %	2644.590	37.22 %	2585.934	38.61 %	2694.873	36.02 %	2816.796	33.13 %	2664.152	36.75 %
	0.33 %	2984.129	29.16 %	2938.004	30.25 %	2969.292	29.51 %	3099.484	26.42 %	2973.439	29.41 %
	0.45 %	3219.946	23.56 %	3235.392	23.19 %	3165.237	24.86 %	3274.870	22.26 %	3172.207	24.69 %
	0.57 %	3496.931	16.98 %	3602.958	14.47 %	3391.135	19.50 %	3484.073	17.29 %	3391.945	19.48 %
Percent of ultimate load of specimens with varied ρ_{web} to the ultimate load of the beam without openings											
Effect of web reinforcement ratio (ρ_{web})	0.24 %	3112.890	26.10 %	3216.231	23.65 %	3090.245	26.64 %	3131.384	25.66 %	3129.490	25.71 %
	0.26 %	3178.988	24.53 %	3227.263	23.08 %	3117.048	26.00 %	3210.752	23.78 %	3139.404	25.47 %
	0.29 %	3219.946	23.56 %	3235.392	23.19 %	3165.237	24.86 %	3274.870	22.26 %	3172.207	24.69 %
	0.33 %	3304.245	21.56 %	3373.015	19.93 %	3270.834	22.35 %	3343.893	20.62 %	3181.053	24.48 %

Where P_u: ultimate load.
P_{us}/P_{uo}: the ratio of ultimate load for studied beams with openings compared to the reference beam without openings.

kN, and 2049.777 kN, respectively. For an opening size of 0.4H (800 mm), the ultimate loads for G1-O8-11, G2-O8-11, and G3-O8-11 were 2197.990 kN, 1551.810 kN, and 1392.245 kN, respectively. Similar to series 1 and 2, the results of series 3 demonstrate that the ultimate load ratio (P_{uo}/P_{us}%) improves with increasing shear span-to-height ratio (a/H) for all opening sizes due to the minor effect of the web opening on the ultimate load ratio (P_{uo}/P_{us}%) for a greater shear span-to-height ratio (a/H). The specimens with a smaller shear span-to-height ratio (a/H) = 0.25 showed a lower ultimate load ratio due to the significant effect of the web opening on decreasing the capacity of RC deep beams with a smaller shear span-to-height ratio (a/H). Table 6 shows that for an opening size of 0.2H (400 mm) and shear span-to-height ratio (a/H) of 0.25, 0.5, and 0.75, the ultimate load ratios (P_{uo}/P_{us}%) for G1-O4-4, G2-O4-4, and G3-O4-4 are 68.21 %, 75.24 %, and 82.49 %, respectively. For an opening size of 0.3H (600 mm) and shear span-to-height ratio (a/H) of 0.25, 0.5, and 0.75, the ultimate load ratio (P_{uo}/P_{us}%) for G1-O6-11, G2-O6-11, and G3-O6-11 is 34.00 %, 51.36 %, and 61.37 %, respectively. Moreover, for an opening size of 0.4H (800 mm) and shear span-to-height ratio (a/H) of 0.25, 0.5, and 0.75, the ultimate load ratios (P_{uo}/P_{us}%) for G1-O8-11, G2-O8-11, and G3-O8-11 were 29.99 %, 34.64 %, and 41.68 %, respectively. The results prove that the ultimate load ratio of beams improves with the opening compared to the ultimate load of beams without openings (P_{uo}/P_{us}%). The reason is that the opening intersects the load path between the loading plate and bearing plate, which decreases the ultimate load more than in the cases of beams with a greater shear span-to-height ratio (a/H = 0.75).

5.1.2. Effect of the concrete compressive strength ($f_c^{'}$)

The 297 specimens in series 1, 2, and 3 were simulated to examine the effect of the concrete compressive strength ($f_c^{'}$) on the ultimate load of the studied beams. Figs. 4, 5, and 9 show the relationship between ultimate load and opening location for specimens in series 1, 2, and 3 to investigate the effect of the concrete compressive strength ($f_c^{'}$) on the ultimate load. Figs. 4, 5, and 9 clearly show that an increase in concrete compressive strength increases the ultimate load of the tested beams. This increase can be described as a uniform increase through identical conditions of the tested beams. This finding is also confirmed by the results in Tables 4-6.

5.1.3. Series 4: Effect of the main reinforcement ratio

Approximately 20 specimens were tested to study the effect of the main reinforcement ratio on the ultimate load of the beams with the following conditions: a concrete compressive strength $f_c^{'}$ of 40 N/mm^2 and a web reinforcement ratio (ρ_{web}) of 0.29 %. Table 7 tabulates the results of the tested specimens in this series. Table 7 shows that specimens with a larger main reinforcement ratio (ρ_s) showed greater ultimate load and ultimate load ratio (P_{uo}/P_{us}%). The ultimate load gained by increasing the main reinforcement ratio (ρ_s) from 0.45 % to 0.57 % was 367.566 kN, which represents 11.36 % for specimen S4-O4-7-ρ_s 0.45 % compared to specimen S4-O4-7-ρ_s 0.57 %. Additionally, the decrease in ultimate load became 14.47 % for the specimen withρ_s = 0.57 % after it was 23.19 % for the specimen withρ_s = 0.45 %. Table 7 shows that a higher ultimate load reduction occurs for beams with smaller main reinforcement ratios (ρ_s). This finding can be explained by the dowel action of the main reinforcement resisting the shear failure of the investigated beams. Beam S4-O4-7 withρ_s = 0.21 % showed the lowest ultimate load among the investigated specimens in series 4. The reason is that beam S4-O4-7-ρ_s 0.21 % has a distribution of the main reinforcement on two rows, which results in less longitudinal reinforcement control around openings due to the increase in distance between the main reinforcement and the opening point. Therefore, increasing the distance from the main reinforcement to the opening is the main reason for decreasing the ultimate load.

5.1.4. Series 5: Effect of the web reinforcement ratio

This series includes 15 tested specimens with identical conditions: concrete compressive strength $f_c^{'}$ of 40 N/mm^2 and main reinforcement ratio (ρ_s) of 0.45 %. The web reinforcement around the opening carries the generated upper path. The current finding is consistent with the study by Hu and Tan [2]. Table 7 shows that decreasing the spacing between web bars enhances the ultimate load by 3.26 % for specimen S5-O4-7-ρ_{web} 0.33 % compared to specimen S5-O4-7-ρ_{web} 0.29 %. The decrease in ultimate load became 19.93 % for specimen S5-O4-7-ρ_{web} 0.33 % after it was 23.19 % for specimen S5-O4-7-ρ_{web} 0.29 % due to the excellent control of web bars around openings for a larger web reinforcement ratio (ρ_{web}). Additionally, the effect of the web reinforcement ratio is insignificant in enhancing the decrease in ultimate load.

5.2. Effect of the opening on the mid-span deflection

The effect of the opening on the mid-span deflection is presented in this section. Specimens with the most critical opening locations were chosen from the analyzed beams in series 2. Those specimens with opening locations 4, 7, 9, 10, and 11 showed the most significant reduction of the ultimate load among the investigated beams.

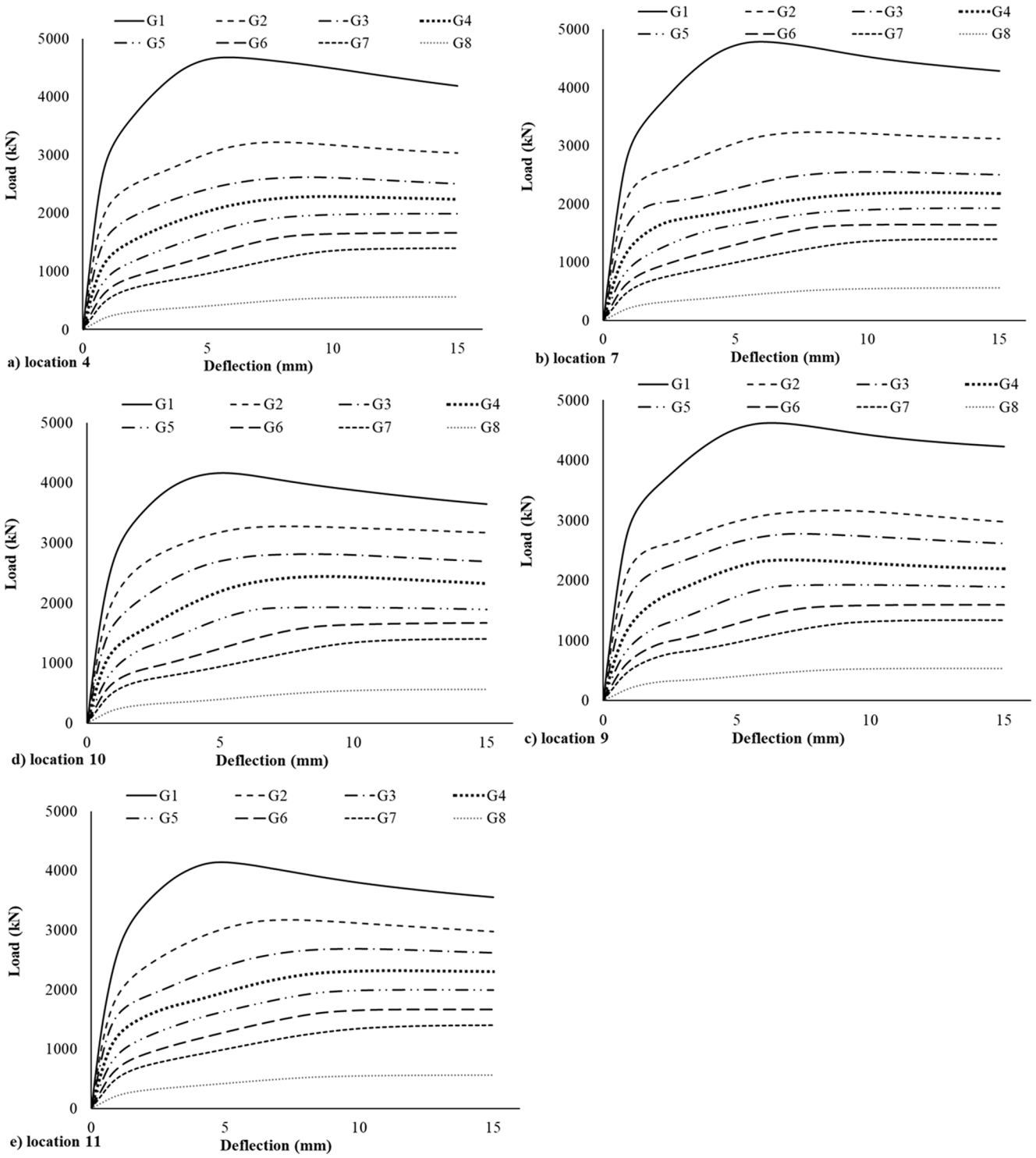

Fig. 10. Effect of the shear span-to-height ratio (a/H) on the load and mid-span deflection of the beams in series 2, O4.

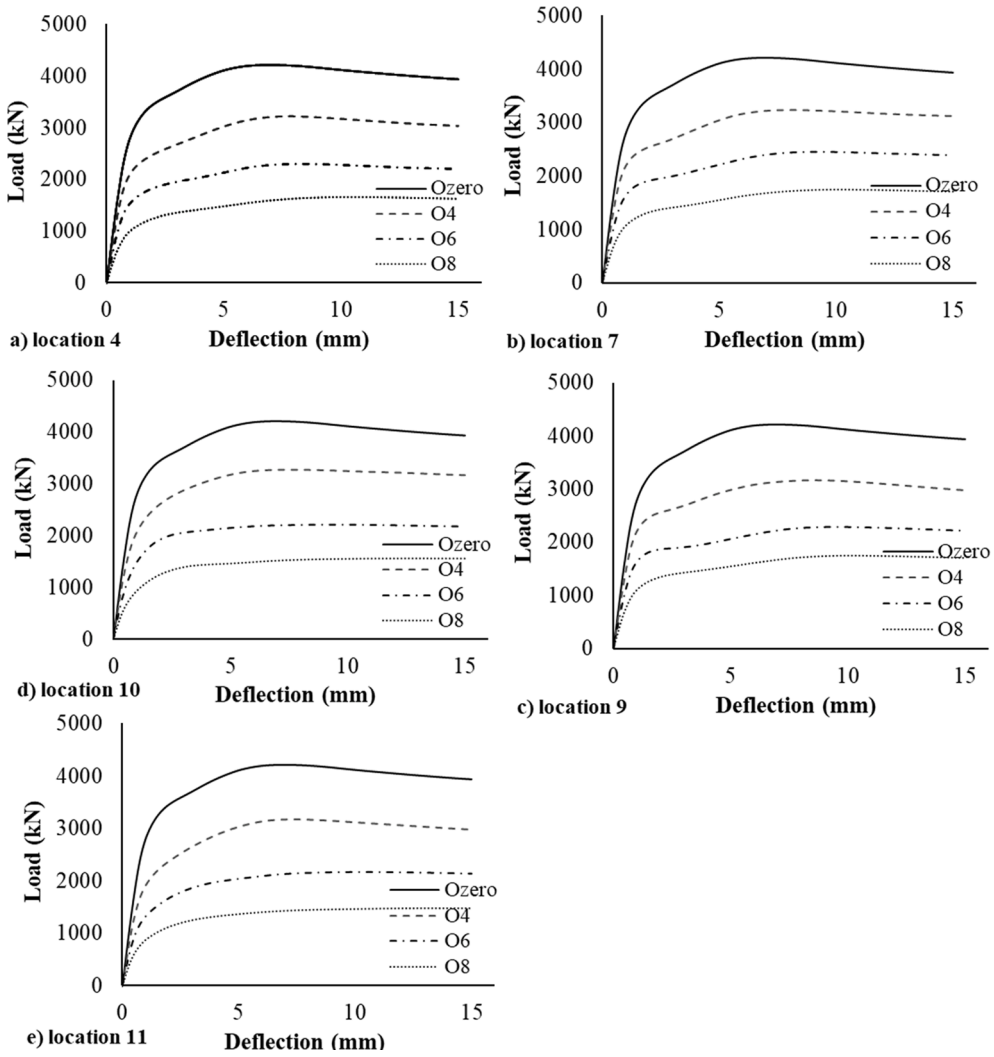

Fig. 11. Effect of the opening on the load and mid-span deflection of the beams in series 2.

5.2.1. Effect of the shear span-to-height ratio (a/H)

Fig. 10 compares the numerical results for the load and mid-span deflection curves, and it shows that a greater shear span-to-height ratio (*a/H*) corresponds to a larger deflection for the beams in series 2, which have identical concrete compressive strength ($f_c^{'}$) and opening size. Moreover, the observed load and mid-span deflection curve of specimen G1-O4-11, which has the smallest shear span-to-height ratio (*a/H*), remain linear until the load reaches almost 2950 kN, which represents 71 % of the ultimate load. The load and mid-span deflection curves of specimens G2-O4-11, G3-O4-11, G4-O4-11, G5-O4-11, G6-O4-11, G7-O4-11, and G8-O4-11, remain linear until the load reaches almost 2000, 1500, 1200, 1000, 800, 560 and 200 kN, respectively, representing 63 %, 56 %, 52 %, 50 %, 48 %, 40 % and 36 % of the ultimate load, respectively. Location 10 in Fig. 10 (d) showed similar behavior to location 11. For the other three locations, 4, 7, and 9, the load and mid-span deflection curves were presented in Fig. 10 (a), (b), and (c), respectively.

5.2.2. Effect of the opening size and location

Fig. 11 shows the effect of the opening size on the relationship between the applied load and mid-span deflection curve. The specimens with larger openings showed higher deflection at the same load. For specimens G2-O4-4, G2-O6-4, and G2-O8-4, the load-deflection curve remains linear until the load reaches almost 2000, 1500, and 1000 kN, respectively, which represents 62 %, 65 %, and 60 % of the ultimate load for those beams, respectively. The load and mid-span deflection curve of specimens G2-O4-7, G2-O6-7, and G2-O8-7 remain linear until the load reaches almost 2000, 1550, and 1000 kN, respectively, which represents 62 %, 63 %, and 57 % of the ultimate load for those beams, respectively. Fig. 11 (c) shows that the load and mid-span deflection curve remains linear until the load reaches almost 2100 kN, 1600 kN, and 1050 kN, representing 66 %, 70 %, and 60 % of the ultimate load for those beams, respectively. The load and mid-span deflection curve of specimens G2-O4-10, G2-O6-10, and G2-O8-10 remain linear until the load reaches almost 2000, 1500, and 600 kN, respectively, representing 61 %, 68 %, and 38 % of the ultimate load for those beams, respectively. Moreover, for specimens with location 11, the load and mid-span deflection curve remains linear until the load reaches almost 1900, 1250, and 750 kN, which represents 60 %, 58 %, and 51 % of the ultimate load for those beams, respectively. Finally, the effect of the opening size on the load and mid-span deflection curve is greater than the influence of the opening location.

5.2.3. Effect of the compressive strength

The effect of the concrete compressive strength ($f_c^{'}$) on the load and mid-span deflection curve of specimens G2-O4-4, G2-O4-7, G2-O4-9, G2-O4-10, and G2-O4-11 is presented in Fig. 12. Thus, an increase in concrete compressive strength ($f_c^{'}$) results in a lesser mid-span deflection. However, the concrete compressive strength ($f_c^{'}$) has a weaker effect on the load and mid-span deflection curve than the other studied

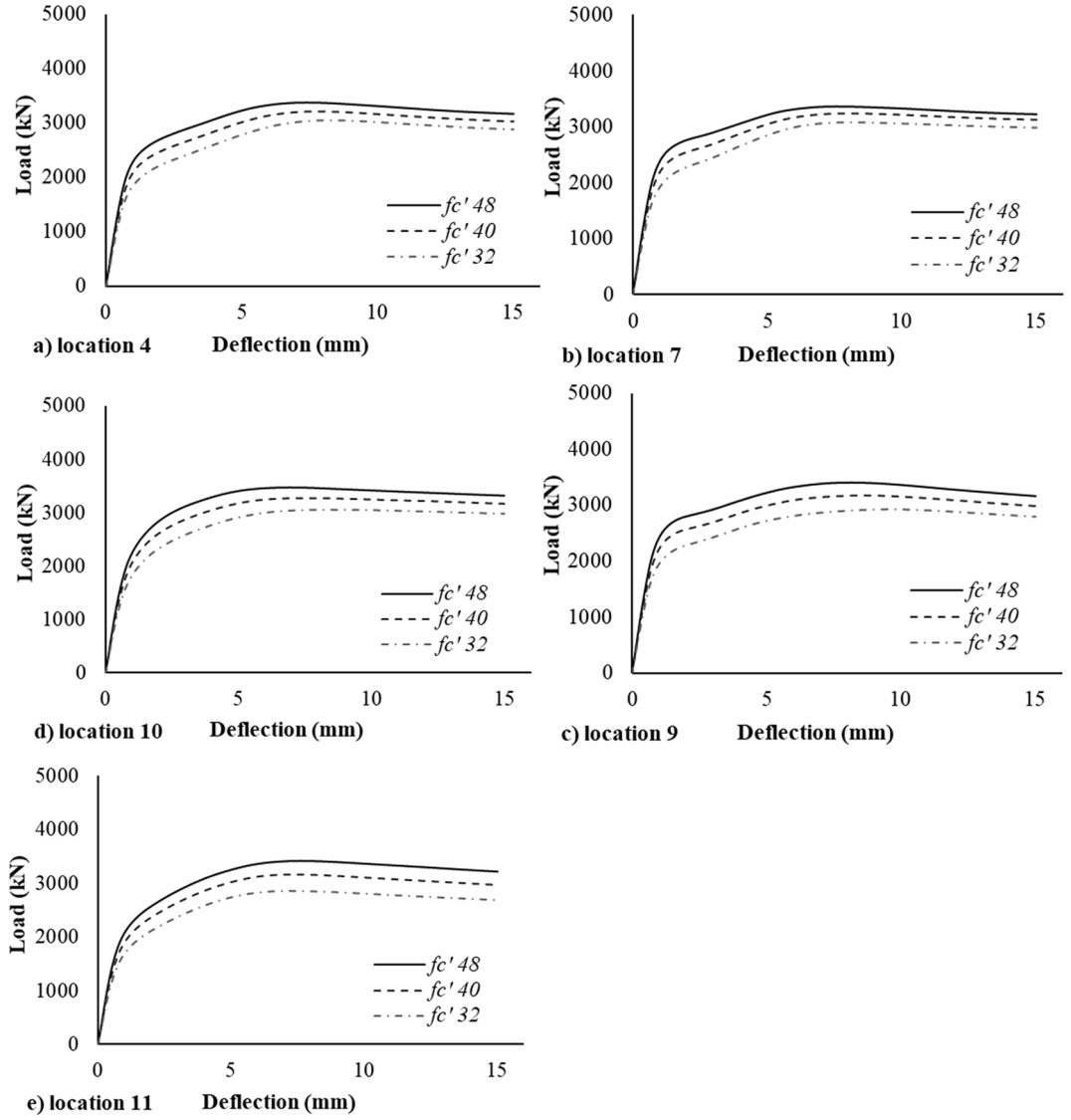

Fig. 12. Effect of the concrete compressive strength ($f_c^{'}$) on the load and mid-span deflection of the beams in series 1, 2, and 3 - O4.

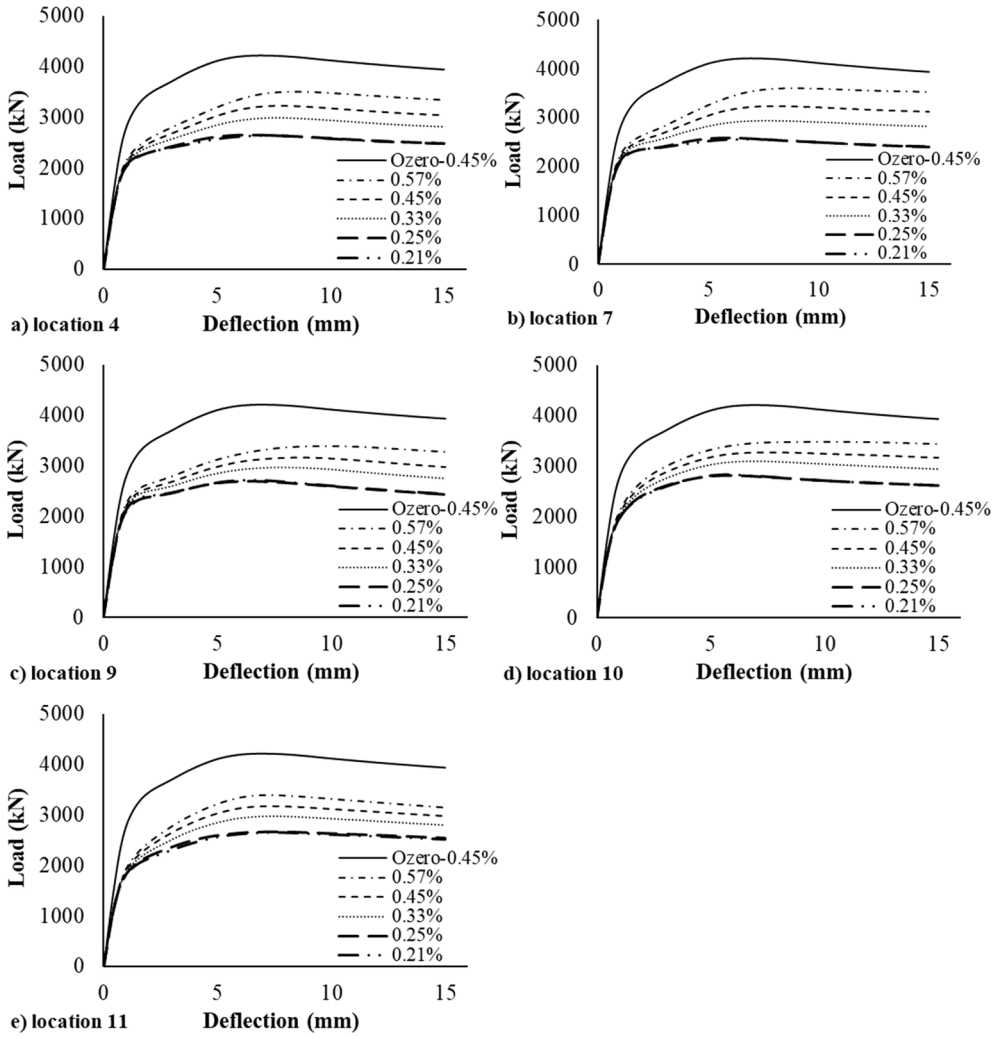

Fig. 13. Effect of the main reinforcement ratio (ρ_s) on the load and mid-span deflection of beams in series 4.

parameters. Fig. 12 (a) presents the relationship between load and mid-span deflection curve of specimens with location 4. The curve remains linear until the load reaches almost 1900, 2000, and 2250 kN, which represents 62 %, 62 %, and 67 % of the ultimate load for those beams with $f_c^{'}$ = 32, 40, and 48 N/mm^2, respectively. For G2-O4-7, the load–deflection curve remains linear until the load reaches almost 2000, 2250, and 2500 kN, which represents 65 %, 70 %, and 74 % of the ultimate load for those beams with $f_c^{'}$ = 32, 40, and 48 N/mm^2, respectively. The load and mid-span deflection curve of specimens with location 9 is linear until the load reaches almost 1900, 2300, and 2500 kN, respectively, which represents 65 %, 73 %, and 74 % of the ultimate load for those beams with $f_c^{'}$ = 32, 40, and 48 N/mm^2, respectively. For G2-O4-10, the load–deflection curve remains linear until the load reaches almost 1750, 2000, and 2300 kN, which represents 57 %, 61 %, and 66 % of the ultimate load for those beams with $f_c^{'}$ = 32, 40, and 48 N/mm^2, respectively. Finally, Fig. 12 (e) shows that the load and mid-span deflection curve remains linear until the load reaches almost 1500, 1900, and 2000 kN, which represents 52 %, 60 %, and 59 % of the ultimate load for those beams with $f_c^{'}$ = 32, 40, and 48 N/mm^2, respectively.

5.2.4. Effect of the main reinforcement ratio

Fig. 13 describes the effect of the main reinforcement ratio (ρ_s) on the load and mid-span deflection curve of specimens S4-O4-4, S4-O4-7, S4-O4-9, S4-O4-10, and S4-O4-11. From the figure, increasing the main reinforcement ratio decreases the deflection. Most of the load and mid-span deflection curves of the studied beams remain linear until the load reaches approximately 57–80 % of the ultimate load.

5.2.5. Effect of the web reinforcement ratio

Fig. 14 presents the effect of the web reinforcement ratio on the relationship between load and mid-span deflection of specimens S5-O4-4, S5-O4-7, S5-O4-9, S5-O4-10, and S5-O4-11. Hence, increasing the web reinforcement ratio decreases the deflection. However, the effect of the web reinforcement ratio on the load and mid-span deflection curve is insignificant. Most load and mid-span deflection curves of the studied beams remain linear until the load reaches approximately 60–71 % of the ultimate load.

5.3. Effect of the opening on the crack pattern and cracking load

This section describes the effect of the opening on the crack pattern and cracking load. The examined specimens are selected from series 2. G2-Ozero is the reference beam without an opening. In this section, specimens G2-O4-4, G2-O4-7, G2-O4-9, G2-O4-10, and G2-O4-11 are analyzed for variation in the opening location. Specimens G2-O6-11 and G2-O8-11 are analyzed to vary in opening size. The crack patterns for the beams at the initiation, ultimate load, and failure are shown in Figs. 15 and 16. A comparison of those figures shows that the cracks start first around the opening and are subsequently followed by cracks in the beam. Afterward, cracks propagate through the load path in the struts

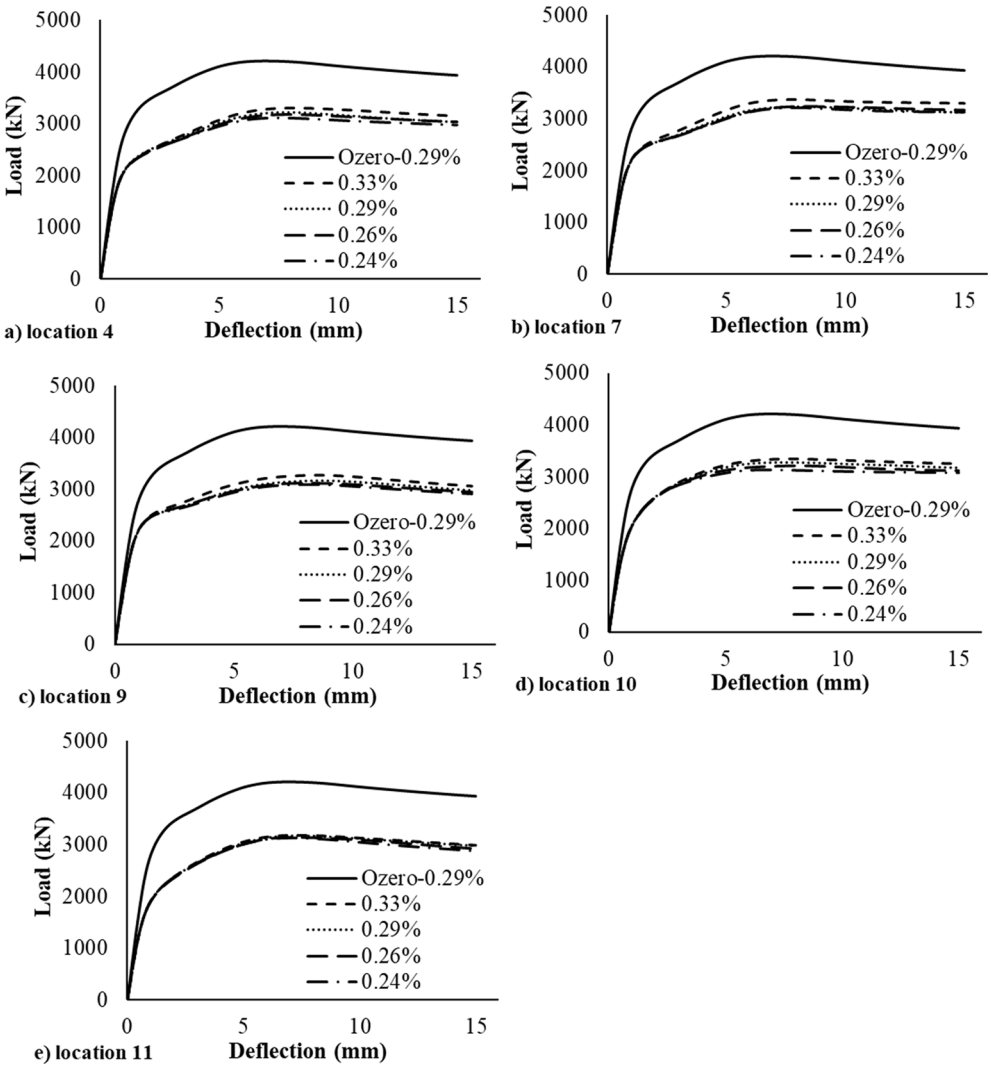

Fig. 14. Effect of the web reinforcement ratio (ρ_{web}) on the load and mid-span deflection of the beams in series 5.

that join the bearing plates with loading points around the opening until failure. Observing the crack patterns in the figures, specimens with larger openings show a higher concentration of shear cracks at the corner of the opening on the load-path line. For beams with smaller opening sizes, cracks spread around all corners of the opening. Thus, beams with a larger opening decrease more in capacity. The cracking loads around the opening and in the beams and their ratio compared to the ultimate load are given in Table 8 for various opening locations. The comparison in Table 8 shows that the beams with an opening near the bearing plate (G2-O4-11) have the smallest cracking load around the opening and in the beam due to high stresses concentrated at the opening. Moreover, Table 8 shows that increasing the opening size decreases the first cracking load (see Fig. 17).

Fig. 15 shows the crack pattern of specimen G2-Ozero at initiation, ultimate load, and failure. Fig. 15 (a) clearly shows that cracks first appear in the beam near the bearing plate through the load path. Table 8 reveals that the first cracking load is 3750.676 kN, which represents 89.04 % of the ultimate load. Then, the cracks began to spread through the line from the loading point to the bearing point, as shown in Fig. 15 (b).

5.3.1. Case 1: Effect of the opening location

The crack patterns of specimen G2-O4-4 at initiation, ultimate load, and failure are shown in Fig. 16.1. Fig. 16.1 (a) shows that cracks initiate at the right-bottom corner of the opening, which is followed by their occurrence in the left-top corner of the opening. The first cracking load is 2130.579 kN, which represents 66.17 % of the ultimate load. Fig. 16.1 (b) shows that the cracks at the beam appear below the opening near the bearing plate through the load path. The cracking load for the beam is 2581.3 kN, representing 80.2 % of the ultimate load. Then, cracks begin to spread through the load path, as clearly shown in Figs. 16.1 (c) and (d). All obtained cracking loads for the studied beams are given in Table 8.

Fig. 16.2 presents the crack pattern of specimen G2-O4-7 at initiation, ultimate load, and failure. Fig. 16.2 (a) shows that cracks simultaneously start at the right-bottom corner and left-top corner of the opening. The observed cracking load is 2530.415 kN, which represents 78.21 % of the ultimate load. Fig. 16.2 (b) shows that cracks at the beam appear below the opening through the load path. The cracking load when cracks begin to appear in the beam is 2720.617 kN, which represents 84.09 % of the ultimate load. Then, cracks begin to spread through the load path, as clearly observed in Figs. 16.2 (c) and (d).

The crack patterns of specimen G2-O4-9 at initiation, ultimate load, and failure are presented in Fig. 16.3. Similar to specimens G2-O4-4 and G2-O4-7, Fig. 16.3 (a) shows that the cracks initiate at the right-bottom corner of the opening. The first cracking load is 2534.8 kN, which represents 80.1 % of the ultimate load. However, unlike specimens G2-O4-4 and G2-O4-7, specimen G2-O4-9 appears to have cracks at the beam above the opening through the load path, as shown in Fig. 16.3 (b). The cracking load when cracks first appear in the beam is 2633.8 kN, which

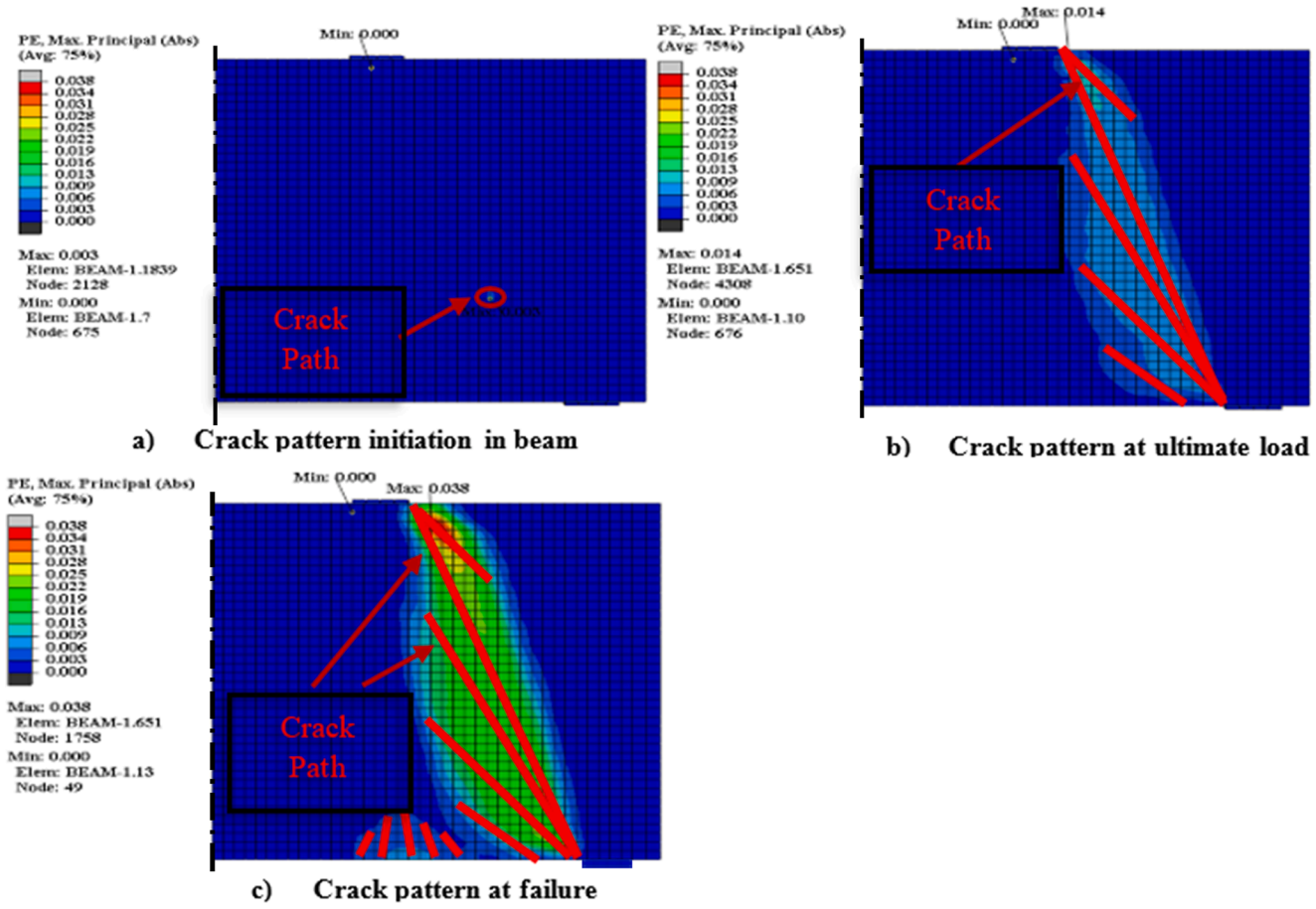

Fig. 15. Crack pattern for G2-Ozero – series 2.

represents 83.2 % of the ultimate load. Then, cracks begin to spread through the load path, as observed in Figs. 16.3 (c) and (d).

Fig. 16.4 presents the crack patterns of specimen G2-O4-10 at initiation, ultimate load, and failure. The cracks for specimen G2-O4-10 initiate at the left-top corner of the opening and subsequently at the right-bottom corner of the opening (as shown in Fig. 16.4 (a)). The first cracking load is 2399.6 kN, which represents 73.3 % of the ultimate load. Fig. 16.4 (b) shows that cracks at the beam appear below the opening near the bearing plate through the load path. The cracking load at the beginning of appearance at the beam is 2920.157 kN, representing 89.17 % of the ultimate load. Then, cracks begin to spread through the load path, as clearly shown in Figs. 16.4 (c) and (d).

Finally, Fig. 16.5 shows the crack pattern of specimen G2-O4-11 at initiation, ultimate load, and failure. Fig. 16.5 (a) shows that cracks start in the left-top corner of the opening for this specimen. The first cracking load is 1864.309 kN, which represents 58.77 % of the ultimate load. Fig. 16.5 (b) shows that cracks at the beam appear below the opening near the bearing plate through the load path. The cracking load when cracks begin to appear in the beam is 2243.803 kN, which represents 70.73 % of the ultimate load. Then, cracks begin to spread through the load path, as shown in Figs. 16.5 (c) and (d).

5.3.2. *Case 2: Effect of the opening size*

The crack patterns of specimen G2-O6-11 at initiation, ultimate load, and failure are exhibited in Fig. 17.1. Fig. 17.1 (a) shows that cracks start at the left-top corner of the opening, and the first cracking load is 1548.8 kN, which represents 71.4 % of the ultimate load. Fig. 17.1 (b) shows that cracks at the beam appear below the opening near the bearing plate through the load path. The cracking load for the beam was 1778.3 kN, representing 82.0 % of the ultimate load. Then, cracks begin to spread through the load path, as shown in Figs. 17.1 (c) and (d). All obtained cracking loads for the studied beams are given in Table 8.

Moreover, Fig. 17.2 shows the crack patterns of specimen G2-O8-11 at initiation, ultimate load, and failure. Fig. 17.2 (a) shows that cracks start in the left-top corner of the opening with the first cracking load of approximately 1119.1 kN, representing 75.7 % of the ultimate load. Fig. 17.2 (b) shows that cracks at the beam appear above the opening through the load path. The cracking load at the beginning of appearance at the beam was 1306.7 kN, representing 88.4 % of the ultimate load. Then, cracks begin to spread through the load path, as shown in Figs. 17.2 (c) and (d).

5.4. *Summary of discussion*

A simulation of the tested beams shows that decreasing the shear span-to-height ratio increases the ultimate load. Meanwhile, increasing the concrete compressive strength increases the ultimate load. The behavior of RC deep beams with web openings mainly depends on the size and location of the openings. Openings cause a considerable reduction in the ultimate load, especially openings with sizes of 0.3 and 0.4 of the overall height of the beam (600 mm and 800 mm). Openings through the shear zone have significant ultimate load reduction, especially openings on the load path and near the bearing plates. With a greater increase in main and web reinforcement ratios, the ultimate load will increase by 11.36 % and 3.26 %, respectively. The numerical results also reveal that greater shear span-to-height ratio (a/H) and opening size correspond to a faster mid-span deflection rate at the same load value. Conversely, increasing the concrete compressive strength (f_c'), main reinforcement ratio (ρ_s), and web reinforcement ratio (ρ_{web}) decreases the mid-span deflection value. Moreover, the effect of the web

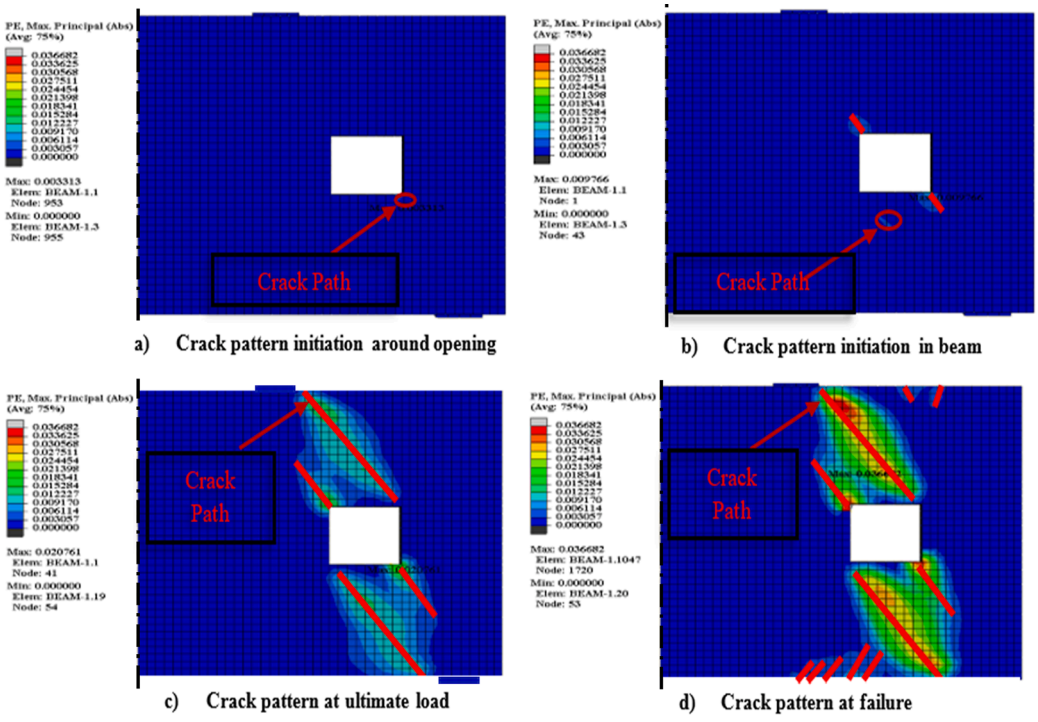

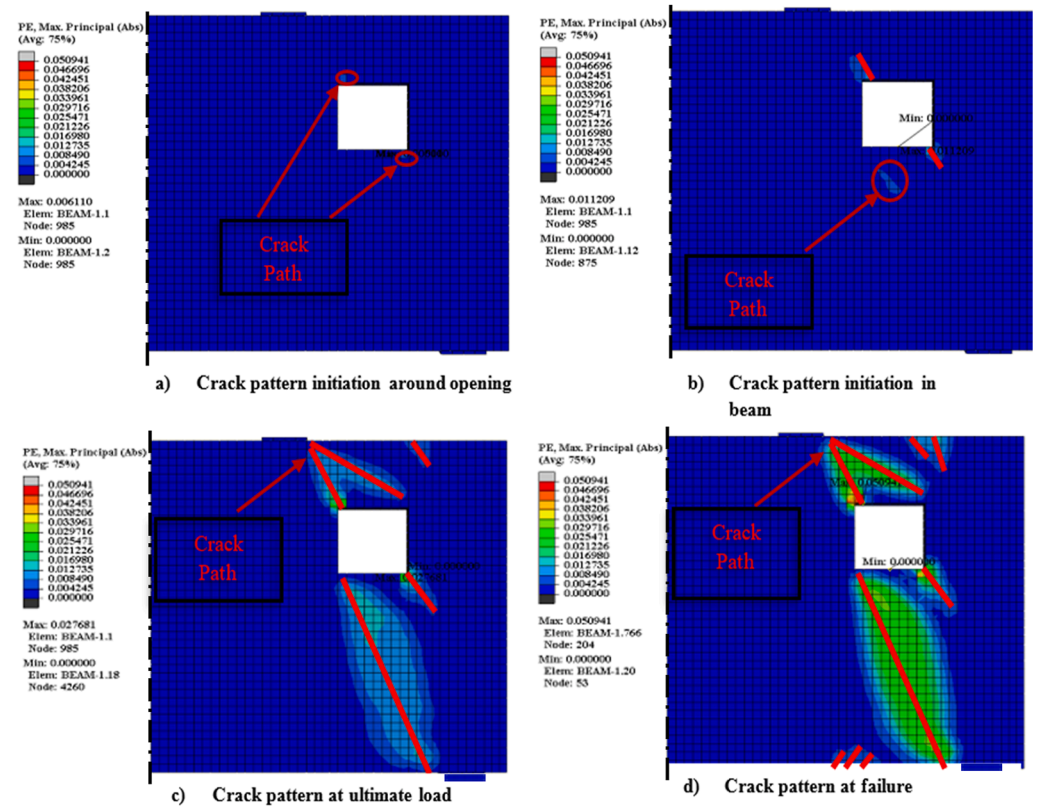

Fig. 16. Case 1: Crack patterns for various opening locations.

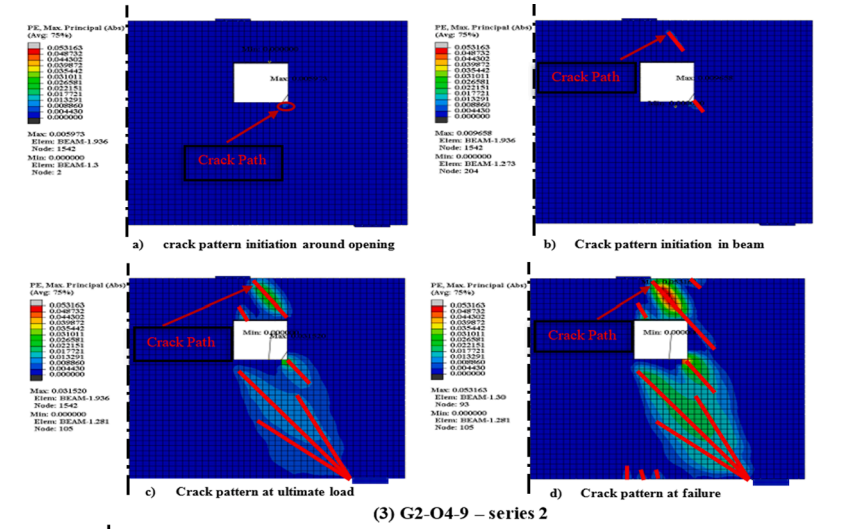

(3) G2-O4-9 – series 2

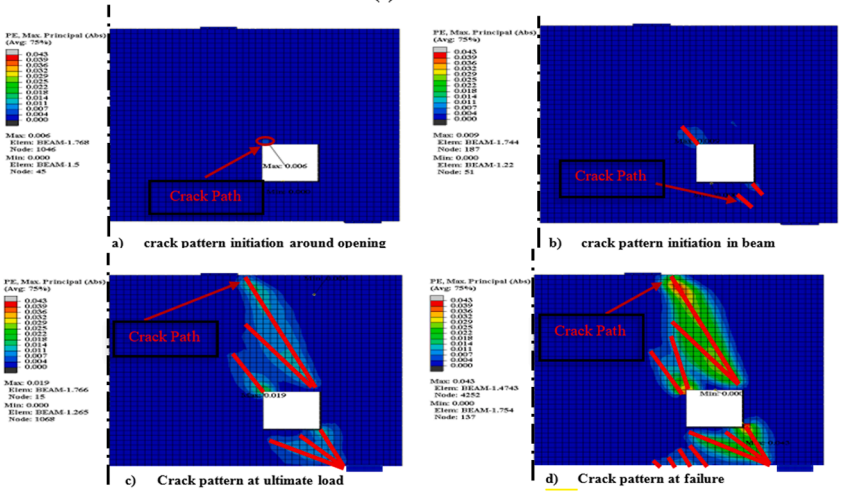

(4) G2-O4-10 – series 2

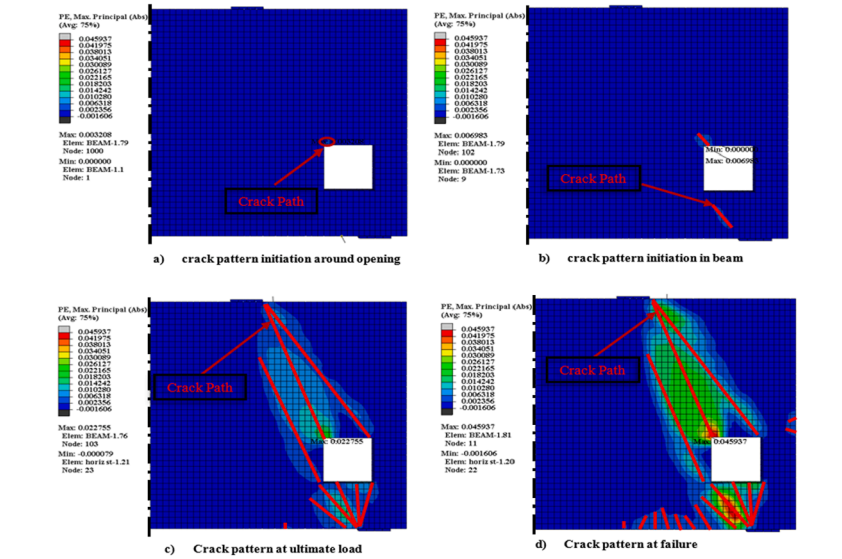

(5) G2-O4-11 – series 2

Fig. 16. (*continued*).

Table 8
Cracking loads for various opening locations and opening sizes.

Comparison case	specimen		P_{cr} initiation at opening (kN)	P_{cr} initiation at opening/P_u	P_{cr} initiation in beam (kN)	P_{cr} initiation in beam/P_u	P_u (kN)
Case 1	Series	Ozero	–	–	3750.676	89.04 %	4212.348
Cracking loads for various opening locations	2	G2-O4-4	2130.579	66.17 %	2581.316	80.17 %	3219.946
		G2-O4-7	2530.415	78.21 %	2720.617	84.09 %	3235.392
		G2-O4-9	2534.763	80.08 %	2633.778	83.21 %	3165.237
		G2-O4-10	2399.618	73.27 %	2920.157	89.17 %	3274.87
		G2-O4-11	1864.309	58.77 %	2243.803	70.73 %	3172.207
Case 2		G2-O4-11	1864.309	58.77 %	2243.803	70.73 %	3172.207
Cracking loads for various opening sizes		G2-O6-11	1548.843	71.42 %	1778.319	82.00 %	2168.774
		G2-O8-11	1119.144	75.69 %	1306.749	88.37 %	1478.664

P_u: ultimate load.
P_{us}/P_{uo}: ratio of the ultimate load for the studied beams with openings compared to the reference beam without openings.

reinforcement ratio (ρ_{web}) on the ultimate load and mid-span deflection of RC deep beams with web openings is insignificant compared to other studied parameters in this study.

For all studied beams, cracks initiate around the opening, followed by the appearance of cracks in the beam. Then, cracks propagate through the loading path in the struts that join the bearing plates with loading points around the opening until failure. Observing the crack pattern, cracks tend to spread around all corners of the opening in specimens with smaller opening sizes. Beams with larger openings show a higher concentration of shear cracks at the corner of the opening on the load-path line. Thus, a more significant decrease in beams' capacity with larger openings is observed.

6. Conclusion

Based on the current study and corresponding theoretical results concerning the structural behavior of reinforced concrete (RC) deep beams with web openings subjected to two-point symmetric top loading, the following conclusions are drawn:

1. The numerical results of the validated specimens were consistent with the experimental work. Therefore, the numerical model can precisely express the behavior of RC deep beams.
2. The behavior of RC deep beams with web openings mainly depends on the openings' size and location. Openings cause a massive reduction in the ultimate load, especially openings with sizes of 0.3 and 0.4 of the overall height of the beam. Moreover, a greater opening size corresponds to a faster rate of mid-span deflection at the same load value. Openings through the flexural zone insignificantly affect the ultimate strength and mid-span deflection. Meanwhile, openings through the shear zone significantly decrease the ultimate strength, especially openings located through the load path near the bearing plates.
3. A more significant increase in the main reinforcement ratio (ρ_s) corresponds to a greater increase in ultimate load and a more considerable decrease in mid-span deflection due to a sufficient resistance to tensile stresses for larger (ρ_s). The enhancement in ultimate load reached 11.36 % for the beam with (ρ_s) of 0.57 % compared to the beam with (ρ_s) of 0.45 %. Moreover, for (ρ_s) of 0.21 %, 0.33 %, and 0.45 %, the steel bars were distributed into two, three, and four rows, respectively. Increasing the distance from the main reinforcement to the opening corner further decreased the ultimate load. That decrease was 39.28 % for beam S4-O4-7-ρ_s 0.21 %.
4. Increasing the spacing between the web reinforcement decreases the ultimate load and increases the mid-span deflection. This is due to adequate cracking control achieved by the bond area around web reinforcement.
5. Based on the numerical results, increasing the concrete compressive strength ($f_c^{'}$) enhanced the beam's resistance against the biaxial stresses generated in intensive concentration below or above the opening.
6. Decreasing the shear span-to-height ratio (a/H) increases the ultimate strength and decreases the mid-span deflection of RC deep beams with web openings. The reason is the significant effect of the flexural behavior for beams with greater (a/H). Otherwise, shear behavior plays a significant role in the beams with lower (a/H) ratios. The shorter shear span dissipates the internal forces and increases the tie-arch action, as proven by the crack propagation of the tested beams.
7. Cracks for all studied beams initiate around the opening, followed by their appearance in other parts of the beam. Cracks propagate through the loading path in the struts that join the bearing plates with loading points around the opening until failure. The observed crack pattern clearly shows that cracks spread around all corners of the opening in specimens with smaller opening sizes, while beams with larger openings showed a higher concentration of shear cracks at the corners of the opening on the load-path line. Thus, a more significant decrease in capacity was observed for beams with larger openings.

Data Availability Statement

All data and models presented in this manuscript are available upon reasonable request to the corresponding author.

CRediT authorship contribution statement

Mona Saleh: Visualization, Methodology, Formal analysis, Validation, Software, Data curation, Writing – original draft. **Mohammad AlHamaydeh:** Conceptualization, Methodology, Formal analysis, Validation, Data curation, Writing – review & editing. **Mohamed Zakaria:** Conceptualization, Methodology, Formal analysis, Validation, Data curation, Writing – review & editing.

Declaration of Competing Interest

The authors declare that they have no known competing financial interests or personal relationships that could have appeared to influence the work reported in this paper.

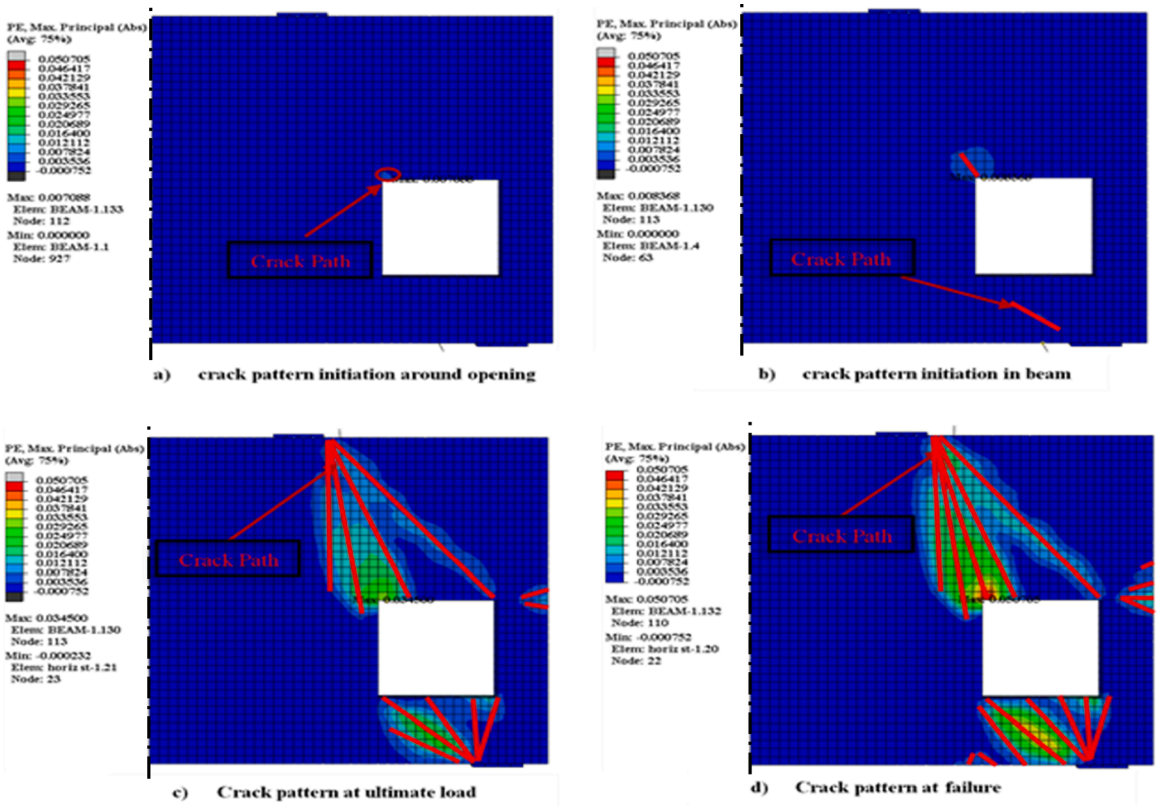

(1) G2-O6-11 – series 2

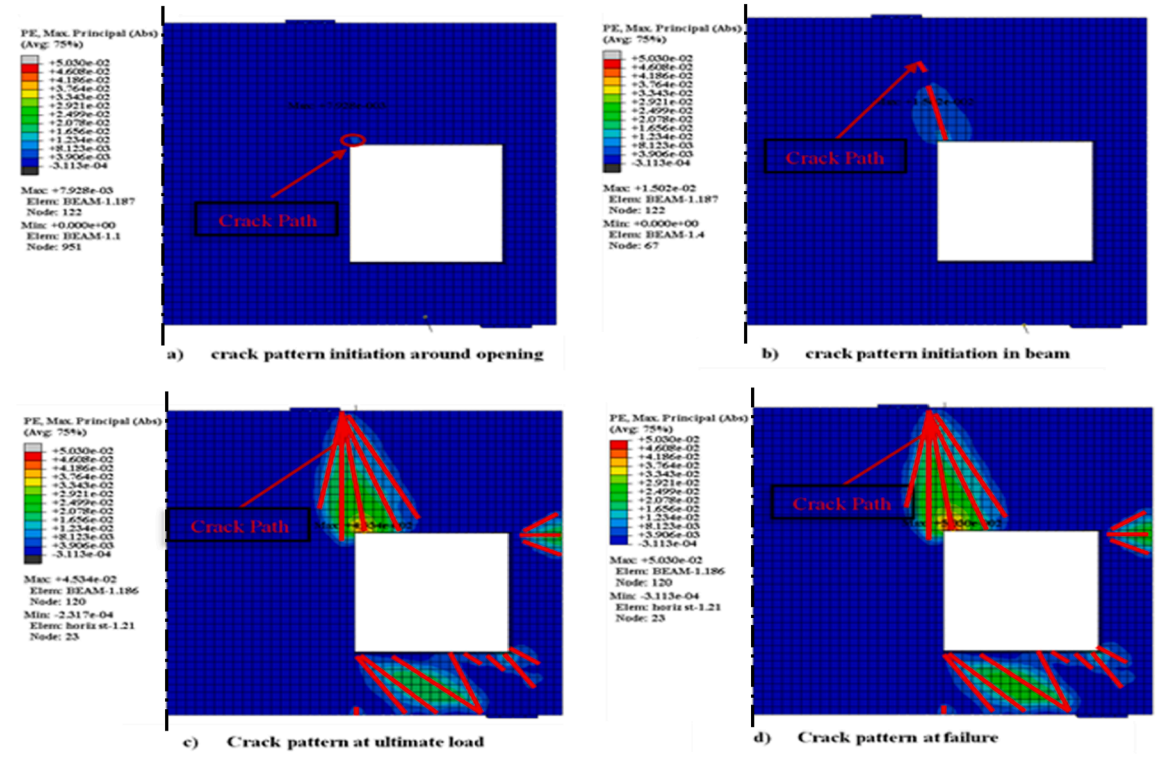

(2) G2-O8-11 – series 2

Fig. 17. Case 2: Crack patterns for various opening sizes.

Data availability

Data will be made available on request.

References

[1] Guan H, Doh J-H. Development of strut-and-tie models in deep beams with web openings. Adv Struct Eng 2007;10(6):697–711.
[2] Hu OE, Tan KH. Large reinforced-concrete deep beams with web openings: test and strut-and-tie results. Mag Concr Res 2007;59(6):423–34.
[3] Zakaria M, Ueda T, Wu Z, Meng L. Experimental investigation on shear cracking behavior in reinforced concrete beams with shear reinforcement. J Adv Concr Technol 2009;7(1):79–96.
[4] Campione G, Minafò G. Behaviour of concrete deep beams with openings and low shear span-to-depth ratio. Eng Struct 2012;41:294–306.
[5] Abdul-Razzaq KS, Ali HI, Abdul-Kareem MM. A new strengthening technique for deep beam openings using steel plates. Int J Appl Eng Res 2017;12(24):15935–47.
[6] Lu W-Y, Lin G-Z, Tseng C-C, Lin S-J. Shear strength of reinforced concrete deep beams with web openings. J Chinese Inst Eng 2020;43(7):694–705.
[7] AlHamaydeh M, Markou G, Bakas N, Papadrakakis M. AI-based shear capacity of FRP-reinforced concrete deep beams without stirrups. Eng Struct 2022;264:114441.
[8] Mabrouk RTS, Mahmoud MAS, Kassem ME. Behavior of reinforced concrete deep beams with openings under vertical loads using strut and tie model. Civ Eng J 2022;7:148–70.
[9] Markou G, AlHamaydeh M. 3D finite element modeling of GFRP-reinforced concrete deep beams without shear reinforcement. Int J Comput Methods 2018;15(02):1850001.
[10] Abed F, El-Chabib H, AlHamaydeh M. Shear characteristics of GFRP-reinforced concrete deep beams without web reinforcement. J Reinf Plast Compos 2012;31(16):1063–73.
[11] Khalil A-HA, Etman EE, EL-Nasr AEA. Behavior of high strength concrete deep beams with openings.
[12] El Maaddawy T, Sherif S. FRP composites for shear strengthening of reinforced concrete deep beams with openings. Compos Struct 2009;89(1):60–9.
[13] Alsaeq HM. Effects of opening shape and location on the structural strength of RC deep beams with openings. Int J Civ Environ Eng 2013;7(6):494–9.
[14] Amin HM, Agarwal VC, Aziz OQ. Effect of opening size and location on the shear strength behavior of RC deep beams without web reinforcement. Int J Innov Technol Explor Eng 2013;3(7):28–30.
[15] Mohamed AR, Shoukry MS, Saeed JM. Prediction of the behavior of reinforced concrete deep beams with web openings using the finite element method. Alexandria Eng J 2014;53(2):329–39. https://doi.org/10.1016/j.aej.2014.03.001.
[16] ACI Committee. Building code requirements for structural concrete (ACI 318-08) and commentary; 2008.
[17] Liu J, Mihaylov B. Shear strength of RC deep beams with web openings based on two-parameter kinematic theory. Struct Concr 2020;21(1):349–61.
[18] Yang K-H, Eun H-C, Chung H-S. The influence of web openings on the structural behavior of reinforced high-strength concrete deep beams. Eng Struct 2006;28(13):1825–34.
[19] Ibrahim MA, El Thakeb A, Mostfa AA, Kottb HA. Proposed formula for design of deep beams with shear openings. HBRC J 2018;14(3):450–65.
[20] Jithinbose KJ, Thomas J, Parappattu NB. Effect of openings in beams – a review. Int J Innov Res Adv Eng 2016;3(9):15–9.
[21] Mansur MA, Alwis WAM. Reinforced fibre concrete deep beams with web openings. Int J Cem Compos Light Concr 1984;6(4):263–71.
[22] Haque M, Rasheeduzzafar, Al-Tayyib AHJ. Stress distribution in deep beams with web openings. J Struct Eng 112(5) (1986) 1147–1165.
[23] K.-H. Yang, H.-S. Chung, A. F. Ashour, Influence of inclined web reinforcement on reinforced concrete deep beams with web openings, 2007.
[24] K.-H. Yang, A.F. Ashour, Effectiveness of web reinforcement around openings in continuous concrete deep beams, 2008.
[25] Coronado CA, Lopez MM. Sensitivity analysis of reinforced concrete beams strengthened with FRP laminates. Cem Concr Compos 2006;28(1):102–14.
[26] A.C.I. Committee, Building code requirements for structural concrete (ACI 318-05) and commentary (ACI 318R-05), 2005.
[27] Gardner NJ. Verification of punching shear provisions for reinforced concrete flat slabs. ACI Struct J 2011;108(5):pp.
[28] Chen GM, Chen JF, Teng JG. On the finite element modelling of RC beams shear-strengthened with FRP. Constr Build Mater 2012;32:13–26.
[29] Martinez J, Jeffers AE. Elevated-temperature tension stiffening model for reinforced concrete structures under fire. 10th Int Conf Struct Fire SIF 2018;18:463–70.
[30] Hofstetter G, Mang HA. Computational plasticity of reinforced and prestressed concrete structures. Comput Mech 1996;17(4):242–54.
[31] Bažant ZP, Oh BH. Crack band theory for fracture of concrete. Matériaux Constr 1983;16(3):155–77.
[32] Jenq Y, Shah SP. Two parameter fracture model for concrete. J Eng Mech 1985;111(10):1227–41.
[33] Demir A, Ozturk H, Bogdanovic A, Stojmanovska M, Edip K. Sensitivity of dilation angle in numerical simulation of reinforced concrete deep beams. Sci J Civ Eng 2017;6(1):33–7.
[34] Kong FK. Reinforced concrete deep beams. CRC Press; 1991.
[35] Committee P. ECP-203: 2007-Egyptian Code for design and construction of concrete structures. HBRC, Giza; 2007. E.-203.